学位論文

Modelling study on thermohaline circulation in the Pacific Ocean

（太平洋における熱塩循環の数値モデルによる研究）

平成10年12月 博士（理学）申請

東京大学大学院理学系研究科
地球惑星物理学専攻

辻野博之

Modelling study on thermohaline circulation in the Pacific Ocean

Hiroyuki Tsujino

Center for Climate System Research, University of Tokyo, Japan

Abstract

Thermohaline circulation in the Pacific Ocean has been investigated by carrying out process-oriented studies using numerical models. Problems in the upper layer, mid-depths, and deep layer in the Pacific are taken up, i.e., the way thermohaline circulation appears in the upper layer, effects of wind forcing on thermohaline circulation at mid-depths, and the role of depth-dependent vertical diffusivity in controlling the deep Pacific circulation.

First, thermohaline effects on the upper layer circulation of the North Pacific is investigated. The Pacific circulation north of 30°S is driven by wind forcing, thermohaline forcing at the sea surface, and Newtonian body forcing at the southern end of the model domain. The three driving agents for the circulation are incorporated step by step into the model to evaluate the role of each agent. The thermohaline forcing at the sea surface enhances the subsurface southward flow, which is the upper part of the layered deep Pacific meridional circulation. This flow suffers distortion but does not disappear, even when the wind forcing is imposed. It follows the eastern and the southern perimeter of the subtropical gyre, becoming the southward western boundary undercurrent at low latitudes. The cross-gyre southward western boundary undercurrent to the tropics, which is indicated in the observed distribution of tracers, is associated with the thermohaline circulation. Thus it is found that at the upper thermocline depths in the subtropical and tropical regions the flows in the poleward and westward region are wind driven, and those in the equatorward and eastward region are thermohaline. The inflow into the tropical South Pacific and South Atlantic of the Antarctic Intermediate Water may be accounted for by this mechanism.

Secondly, effects of wind forcing on thermohaline circulation at mid-depths are investigated. A rectangular ocean which extends over the northern and

southern hemispheres is driven by differential heating and wind stress at the sea surface. The differential heating is so distributed that the deep water is formed at the southern end of the model ocean. The wind stress is so distributed that there are three wind-driven gyres in the northern hemisphere, and it is not imposed in the southern hemisphere. Comparison is made between the cases with and without the wind stress. When the wind forcing is imposed, the basin-scale meridional circulation increases in intensity. This is due to the enhanced surface heating in the cyclonic wind-driven gyre with the Ekman upwelling and the accompanying enhanced surface cooling in the deep water formation region. In the cyclonic wind-driven gyre, the Ekman upwelling brings up the thermocline to the subsurface depths to enhance the surface heating and also the downward heat conduction from the sea surface to the deep layer, which leads to warming of the deep water. Thus, the enhanced surface heating in the cyclonic gyre is balanced with the enhanced surface cooling in the deep water formation region due to the warmed deep water. In this way, the wind forcing enhances thermohaline circulation, wind-enhanced thermohaline circulation, which connects the deep water formation region to the cyclonic wind-driven gyre with the Ekman upwelling.

Finally, deep Pacific circulation is investigated by using an idealized two-basin model. Depth-dependent vertical diffusivity is employed to control the circulation. Vertical diffusivity estimated from observations, $0.1\,\mathrm{cm^2\,s^{-1}}$ and $3.0\,\mathrm{cm^2\,s^{-1}}$, is adopted for the upper layer and for the deep layer, respectively. Comparison is made among cases with different profiles of vertical diffusivity at mid-depths. When vertical diffusivity is set to increase progressively with depth beginning at the lower thermocline depths, the deep circulation is significantly intensified. This is due to enhanced heat exchange between the thermocline water and the deep water through the enhanced diffusion at the lower thermocline depths. The water below the thermocline is warmed and the water above the thermocline is cooled for the whole basin. The warmed deep water leads to enhanced deep water formation in the deep water formation region due to excess heat loss through the sea surface. The cooled upper-layer water leads to excess heat gain through the sea surface, balancing with the excess heat loss in the deep

water formation region. The deep water upwelled to the lower thermocline depths does not further upwell to the sea surface due to the small upper-layer vertical diffusivity, but it flows back to the Southern Ocean, slowly upwelling at the thermocline depths. In this way, the meridional overturning with large transport forms below the lower thermocline in the Pacific. This circulation yields tracer distributions that are well compared with the observation.

When vertical diffusivity larger than $1.0\,\mathrm{cm^2\,s^{-1}}$ is taken in the deep layer, a set of alternating zonal jets, the stacked jets, along the equator is formed by the effect of vertical diffusion. The speed of the stacked jets is the greatest when vertical diffusivity increases with depth beginning at the lower thermocline depths, i.e., when the deep circulation is the most intense.

Acknowledgments

I would like to express my heartfelt gratitude to Professor Nobuo Suginohara for his valuable guidance, stimulating discussions, and continuous encouragements. I would also like to express my thanks to Drs. Ryo Furue, Hiroyasu Hasumi, and Yasuhiro Yamanaka for their fruitful discussions and helpful comments. Thanks are extended to all the members and ex-members of the Ocean Modelling Group, Center for Climate System Research, University of Tokyo, for their helps and pleasant discussions.

The numerical experiments were performed on the HITAC S-3800 at the Computer Center, University of Tokyo. Figures were drawn with graphic routines in GFD-Dennou Library, developed by GFD-Dennou Club.

Contents

Chapter 1

General Introduction

1.1 Thermohaline circulation

Thermohaline circulation in the ocean is driven by the distribution of the heat and freshwater flux through the sea surface. It is considered to take the form that high density water formed by convection in the very narrow region upwells in the rest of the ocean to balance with downward heat conduction from the sea surface (e.g., Suginohara and Aoki, 1991).

The global thermohaline circulation at the present state of climate shows that a large amount of deep and bottom waters formed in the northern North Atlantic and in the marginal seas of the Southern Ocean such as the Weddell Sea upwell in the Indian and the Pacific Ocean (Broecker et al., 1985; Gordon, 1986). It takes about 1500 years for North Atlantic Deep Water (NADW) to close the worldwide circuit during which it is gradually modified toward low density water by slow mixing processes. There also exist thermohaline circulations at the shallower depths closed within each oceanic basin, which are considered to have a time scale of several ten to hundred years. By making a great contribution to meridional heat transport, thermohaline circulation plays an important role in determining the state of the climate. Understanding thermohaline circulation is an essential part in the study of the climate system.

1.2 Thermohaline circulation in the Pacific

In the northern North Pacific, since there occurs no extensive dense water formation that leads to strong thermohaline circulation, it is believed that thermohaline circulation is weak in the upper layer of the North Pacific. The deep and the bottom layer of the Pacific are filled with Circumpolar Deep Water (CDW), which is a mixture of NADW formed in the northern North Atlantic and Antarctic Bottom Water (AABW) formed in the marginal seas of the Southern Ocean. CDW flows into the bottom layer of the Pacific from the Southern Ocean, slowly upwells, and finally returns to the Southern Ocean at mid-depths (Wunsch et al., 1983). According to the radio carbon distribution, the oldest water mass in the world ocean resides in the northern North Pacific around the depth of 2000 m, which confirms that no deep water source exists within the North Pacific and the deep water comes from the other oceans. The general understanding on the state of

thermohaline circulation in the Pacific that is deduced mainly from observational evidence is presented by Schmitz (1995) and Reid (1997).

It cannot be said that much attention has been paid to the thermohaline circulation in the Pacific for modelling the global thermohaline circulation. Every ocean general circulation model (OGCM) produces roughly same results for the Pacific (e.g., Toggweiler et al. 1989; Maier-Reimer et al., 1993; Hasumi and Suginohara, 1998). Although they reproduce the general features of the Pacific circulation, discussion on details of the Pacific thermohaline circulation is rarely found except for Toggweiler and Samuels (1993) and Nakata and Suginohara (1998). This may be due to the fact that the northern North Pacific is not the source region of deep water but is the terminal of the oceanic conveyer belt. However, since thermohaline circulation consists of both formation and subsequent modification of deep water, it is important to investigate the modification process of deep water as well as the formation process to fully understand thermohaline circulation. Besides, thanks to the recent observation conducted by the international projects such as World Ocean Circulation Experiment (WOCE), details of the circulation in the Pacific are becoming clear. As presented below, there are some features that are not found in the existing simulations. Their mechanisms should be clarified. Henceforth, more detailed knowledge about the Pacific circulation obtained by observations will check results of simulations more strictly.

1.3 Objectives and contents of this thesis

Process-oriented study using a numerical model is a very effective way to clarify mechanism governing some oceanic process. This type of study takes advantage of a numerical model that can easily yield a circulation field for a situation where some boundary condition or internal parameter is changed. By contrasting difference among cases with different boundary conditions or parameters, we can clarify principal factors that govern that process. Particularly, this type of study is extremely useful in clarifying mechanism of thermohaline circulation because mathematical treatment of thermohaline circulation is difficult owing to its nonlinearity.

In the present thesis, the thermohaline circulation in the Pacific Ocean is investigated by carrying out process-oriented studies using numerical models. Problems of thermohaline circulation in the upper layer, mid-depths, and deep layer are taken up. In chapter 2, the

way thermohaline circulation appears in the upper layer of the North Pacific is investigated. And it is demonstrated that the meridional circulation at mid-depths is intensified when wind forcing is imposed. Its mechanism is thoroughly investigated in chapter 3. A mechanism which provides a connection between wind forcing and thermohaline circulation is clarified. In chapter 4, the Pacific deep and bottom circulation is investigated. It is demonstrated that depth-dependent vertical diffusivity plays an important role in controlling the circulation. Finally, general conclusion is presented in chapter 5.

References

Broecker, W. S., D. M. Peteet and D. Rind (1985): Does the ocean-atmosphere system have more than one stable mode of operation?, *Nature*, **315**, 21–26.

Gordon, A. L. (1986): Interocean exhange of thermocline water, *J. Geophys. Res.*, **91**, 5037–5046.

Hasumi, H. and N. Suginohara (1998): Sensitivity of a global ocean general circulation model to tracer advection schemes, *J. Phys. Oceanogr*, submitted.

Maier-Reimer, E. M., U. Mikolajewicz and K. Hasselmann (1993): Mean circulation of the Hamburg LSG OGCM and its sensitivity to the thermohaline surface forcing, *J. Phys. Oceanogr.*, **23**, 731–757.

Nakata, M. and N. Suginohara (1998): Role of deep stratification in transporting deep water from the Atlantic to the Pacific, *J. Geophys. Res.*, 1067–1086.

Reid, J. L. (1997): On the total geostrophic circulation of the Pacific Ocean: Flow patterns, tracers, and transports, *Prog. Oceanog.*, **39**, 263–352.

Schmitz, W. J. (1995): On the interbasin-scale thermohaline circulation, *Rev. Geophys.*, **33**, 151–173.

Suginogara, N. and S. Aoki (1991): Buoyancy-driven circulation as horisontal convection on β-plane, *J. Mar. Res.*, **49**, 295–320.

Toggweiler, J. R., K. Dixon and K. Bryan (1989): Simulations of radiocarbon in a coarse-resolution world ocean model 1. Steady state prebomb distributions, *J. Geophys. Res.*, **94**, 8217–8242.

Toggweiler, J. R. and B. Samuels (1993): New radiocarbon constraints on the upwelling of abyssal water to the oceans's surface, in Heimann, M. ed., *The global carbon cycle*, NATO ASI Series, Springer-Verlag, Berlin, 333–366.

Wunsch, C., D. Hu and B. Grant (1983): Mass, Heat, Salt and nutrient Fluxes in the South Pacific Ocean, *J. Phys. Oceanogr.*, **13**, 725–753.

Chapter 2

Thermohaline effects on upper layer circulation of the North Pacific

This chapter is from the published paper by Tsujino and Suginohara (*J. Geophys. Res.*, **103**, 18,665-18,679, 1998).

Abstract

We investigate thermohaline effects on the upper layer circulation of the North Pacific by carrying out numerical experiments. The Pacific circulation north of 30°S is driven by wind forcing, thermohaline forcing at the sea surface, and Newtonian body forcing at the southern end of the model domain. The three driving agents for the circulation are incorporated step by step into the model to evaluate the role of each agent. The thermohaline forcing at the sea surface enhances the subsurface southward flow, which is the upper part of the layered deep Pacific meridional circulation. This flow suffers distortion but does not disappear, even when wind forcing is imposed. It follows the eastern and the southern perimeter of the subtropical gyre, becoming the southward western boundary undercurrent at low latitudes. The cross-gyre southward western boundary undercurrent to the tropics, which is indicated in the observed distribution of tracers, is associated with the thermohaline circulation. Thus it is found that at the upper thermocline depths in the subtropical and tropical regions the flows in the poleward and westward region are wind driven, and those in the equatorward and eastward region are thermohaline. The inflow into the tropical South Pacific and Atlantic of the Antarctic Intermediate Water may be accounted for by this mechanism.

2.1 Introduction

Distributions of tracers such as salinity, oxygen, and nutrients are used as the indicator of flows in the ocean. In the upper layer of the North Pacific there are noticeable two vertical salinity minima: the Shallow Salinity Minima (SSM) and the North Pacific Intermediate Water (NPIW). SSM are the vertical minima of salinity observed in the upper layer ($\sigma_\theta = 25.1 \sim 26.2$) along the eastern and the southern perimeter of the subtropical gyre (Reid, 1973; Yuan and Talley, 1992). Formation regions of SSM are considered to be at the high latitudes (as high as about 50°N) in the eastern North Pacific (see Figure 1 of Reid, 1973) and in the northeastern part of the subtropical gyre (Tsuchiya, 1982; Yuan and Talley, 1992). A low-salinity water at the sea surface at the high latitudes submerges and flows toward the midlatitude region, where a more saline but less dense water overlies, and then the minimum is formed. Talley (1985) studied the formation and the distribution of SSM by using a ventilated thermocline model (Luyten et al., 1983) and pointed out that they are due to the wind-driven, ventilated circulation in the subtropical gyre. But her work does not explain that part of SSM originate from the north of the subtropical gyre (Reid, 1973). SSM disappear before they join the western boundary current, possibly because they are vertically mixed with the saline surface water above.

NPIW is the vertical salinity minimum observed in the subtropical gyre of the North Pacific at density around $\sigma_\theta = 26.8$ (Talley, 1993). A low-salinity water on those density surfaces is considered to be formed in the northwestern part of the subpolar gyre or in the Okhotsk Sea (Talley, 1993; Yasuda et al., 1996; Yasuda, 1997). The minimum itself is formed in the Mixed Water Region east of Japan, where this low-salinity water is brought below the saline but less dense water of the subtropical origin and modified by effects of mesoscale eddies (Talley et al., 1995; Yasuda, 1997). Talley (1988), by mapping potential vorticity distribution, pointed out that NPIW around $\sigma_\theta = 26.8$ is distributed by the wind-driven circulation in the subtropical gyre. But its southern limit is located at 20°N, as can be seen in Talley's (1993) map of salinity distribution on $\sigma_\theta = 26.8$, which is not the southern end of the subtropical gyre. South of 20°N, NPIW is confined to the western boundary region. It seems that NPIW is transported to the tropics by the southward western boundary undercurrent east of the Philippines. A similar flow pattern is indicated by Suga and Talley (1995) for the inflow of the Antarctic Intermediate Water (AAIW) into

the tropics in the South Atlantic.

The distributions of the salinity minima raise two problems about the upper layer circulation of the North Pacific:

I. How are part of SSM formed at the high latitudes north of the subtropical gyre (Reid, 1973), and how are they transported to the subtropical gyre? Is there a southward cross-gyre flow at the eastern subpolar-subtropical gyre boundary?

II. What kind of mechanism brings NPIW to the tropics? Is there really such a western boundary undercurrent east of the Philippines in the southern part of the subtropical gyre?

The upper layer circulation of the middle- and high-latitude North Pacific is, in general, believed to be dominated by wind-driven circulation. Many efforts have been made to explain the circulation of the Pacific within the context of the wind-driven circulation theory. As to problem 1, the low-salinity water crossing the gyre boundary from the subpolar to the subtropical gyre cannot be explained by the ventilated thermocline theory. Although there is a solution with a cross-gyre flow in the wind-driven circulation theory of Chen and Dewar (1993), their solution at the western boundary is rather unrealistic. As to problem 2, McCreary and Lu (1994) showed in a 2.5-layer model that there is a low-latitude southward western boundary current in the second layer. But the second layer, the subducted layer, corresponds to depths shallower than NPIW. Their model cannot be applied to the distribution of NPIW.

As can be understood in the above discussions, the two problems about the cross-gyre flow do not seem to be resolved by the wind-driven circulation theory alone. Of course the Ekman transport and its compensation flow cross the gyre boundary. But their effects do not seem dominant. At the boundary between the subtropical and the subpolar gyre the Ekman transport is southward, and its compensation flow is northward. Thus this pattern does not explain the southward flow of Reid's salinity minimum at that boundary. On the other hand, at the boundary between the subtropical and the tropical gyre the Ekman transport is northward, and its compensation flow is southward, a pattern that does not seem to conflict with the southward spreading of NPIW. But if NPIW is carried into the tropics by the southward compensation flow, we cannot explain the observed fact that

the spreading of NPIW from the subtropical gyre to the tropics is confined to the western boundary region (Talley, 1993). Therefore thermohaline effects are considered important in establishing the cross-gyre flows. Reid and Arthur (1975) showed that the subtropical gyre shifts toward the higher latitudes with increasing depth. Also, the wind-driven circulation theory shows that the subtropical gyre shrinks toward the northwest with increasing depth. Thus it can be considered that thermohaline effects may appear at the subsurface depths along the eastern and the southern perimeter of the subtropical gyre. Since the depths to which effects of the wind forcing reach are considered to become shallower toward the south in the subtropical gyre, NPIW in the southern part of the subtropical gyre may feel the effects of thermohaline forcing. Thus it may not be strange that NPIW takes a flow path in the eastern and the southern part of the subtropical gyre that is not accounted for only by the effects of wind forcing.

For thermohaline circulation in the Pacific there may be two driving agents: the thermohaline forcing that the Southern Ocean exerts on the Pacific and the thermohaline forcing at the sea surface due to the distribution of heat and freshwater fluxes through the sea surface. As to the former, the meridional circulation of the deep Pacific has the layered structure, i.e., the northward flow of the Lower Circumpolar Water near the bottom and the southward return flow at mid-depths (Obata et al., 1996). As to the latter, however, little attention is paid because the winter sea surface density in the high-latitude North Pacific is not larger than $27.0\sigma_\theta$, small enough to indicate that, unlike the North Atlantic, no extensive dense water formation that leads to a strong thermohaline circulation occurs in the North Pacific. However, the observed distributions of the salinity minima in the North Pacific yield characteristics that cannot be explained by the wind-driven circulation theory alone, and the salinity minima themselves are formed by sea surface processes, which indeed include thermohaline convection. These facts may lead to the importance of thermohaline forcing at the sea surface as a driving agent for the upper layer circulation of the North Pacific.

In this chapter, by using a numerical model for the Pacific north of 30°S, we investigate the effects of sea surface thermohaline forcing on the upper layer circulation of the North Pacific. To accomplish this investigation, the three driving agents for the North Pacific circulation, i.e., the thermohaline forcing exerted by the Southern Ocean, the sea surface thermohaline forcing, and the wind forcing, are incorporated step by step. First, a circu-

lation induced by the thermohaline forcing exerted by the Southern Ocean is calculated (case 1). A deep circulation pattern of the North Pacific is formed by creating a buffer region at the southern end of the model domain, where temperature and salinity are restored to the observed values from the sea surface to the bottom, i.e., Newtonian body forcing. Next the sea surface thermohaline forcing is imposed on case 1 (case 2) by restoring sea surface temperature and salinity to the realistic sea surface reference temperature and salinity. A circulation forced only by the thermohaline process is established. Finally, wind forcing is imposed on case 1 (case 3) and also on case 2 (case 4). Case 4 corresponds to simulation of the North Pacific circulation. By comparing the cases the roles of each of the three driving agents are understood. Thus the problems posed above will be resolved.

This chapter is organized as follows. Section 2.2 describes the model. Results of the calculations are presented in section 2.3. Section 2.4 discusses some problems that arise from the formulation adopted in the model. Section 2.5 presents concluding remarks.

2.2 Model

We use the Center for Climate System Research ocean general circulation model (CCSR-OGCM). The CCSR-OGCM is a multilevel model that solves primitive equations under the hydrostatic, the Boussinesq, and the rigid lid approximation. The finite differencing method is the same as that of Suginohara and Aoki (1991). Unstable stratification is removed by convective adjustment: when the potential density of a certain grid point is larger than that just below, potential temperature and salinity are homogenized downward from that grid point until unstable stratification is completely removed. The model domain and the bottom topography are shown in Figure 2.1. Since the region we are interested in is north of the equator, the southern boundary of the model domain is taken to be 30°S, and the zonal band adjacent to the southern boundary is considered the buffer zone, where the Southern Ocean exerts thermohaline forcing on the Pacific. This thermohaline forcing is made by Newtonian body forcing: potential temperature and salinity, and hence density, from the sea surface to the bottom in the zonal band between 20°S and 30°S are restored to the observed values of Levitus' (1982) winter data at 21°S, where the Sverdrup stream function is approximately zero. The damping time is 60 days.

Cases 1 through 4 are listed in Table 2.1. For cases 1 and 3 the sea surface reference

temperature and salinity are set to be constant. The constant values adopted are those that yield the lowest reference density at the sea surface in the body forcing region, i.e., the lowest sea surface density at 21°S of Levitus' (1982) data.

In cases 2 and 4 the reference temperature and salinity for the sea surface thermohaline forcing are taken from Levitus' (1982) winter data. Temperature and salinity at the sea surface are restored to the reference values with a damping time of 60 days. In the Okhotsk Sea the averaged values within the Okhotsk Sea at 100 m depth (−0.33°C, 33.16 psu, and $26.64\sigma_\theta$) are used to reproduce the direct ventilation beneath sea ice (Talley, 1993). In cases 3 and 4 we impose Hellerman and Rosenstein's (1983) wind stresses averaged over February, March, and April north of the equator. The wind stress in the body forcing region (from 20°S to 30°S) is uniform, where the zonally averaged value at 20°S is adopted. Between the equator and 20°S the wind stress is obtained by linearly interpolating the realistic values at the equator and 20°S on each longitude.

The horizontal resolution is 2° × 2°, and there are 40 levels in the vertical with high resolution near the sea surface (50 m) and decreased resolution toward the bottom (200 m). Because the horizontal resolution is coarse, most of the fine structures of the topography such as the Kuril Islands are omitted and smoothed. At the southern end of the model ocean the Tonga Trench is broadened, so that the Lower Circumpolar Water can flow into the North Pacific Basin.

We use the following values for the model parameters: $A_H = 8.0 \times 10^8$ cm^2 s^{-1}, $A_V = 1.0$ cm^2 s^{-1}, $K_H = 1.0 \times 10^7$ cm^2 s^{-1}, and $K_V = 0.3$ cm^2 s^{-1}, where A_H and A_V are the horizontal and the vertical viscosity coefficient and K_H and K_V are the horizontal and the vertical diffusion coefficient. The model equations are integrated for about 3000 years to obtain a thermally and dynamically steady state using Bryan's acceleration method (Bryan, 1984).

2.3 Results

2.3.1 Description of General Features

The vertically integrated mass stream function for case 4 and the Sverdrup stream function calculated from the imposed wind stress are shown in Figures 2.2a and 2.2b, respectively. Hereafter we discuss mainly the results north of the equator. The flow patterns for

Table 2.1: List of Experiments

Case	Wind Forcing	Surface Reference Temperature and Salinity
1	off	uniform
2	off	Levitus (1982)
3	on	uniform
4	on	Levitus (1982)

case 3 (not shown here) are almost the same as those for case 4. In case 4 (Figure 2.2a) there are three wind-driven gyres north of the equator, reflecting the imposed wind stress pattern (Figure 2.2b). We call them from south to north the tropical gyre, the subtropical gyre, and the subpolar gyre. The boundary between the tropical and the subtropical gyre is approximately at 14°N in the western boundary region, which is slightly north of that of the Sverdrup stream function. The boundary between the subtropical and the subpolar gyre is about at 45°N in the eastern region, which is nearly the same as that of the Sverdrup stream function. Though the general feature of the horizontal mass transport stream function north of the equator for case 4 is similar to that of the Sverdrup stream function, there are some differences. The circulation of the subpolar gyre is separated into two gyres. The separation into two gyres of the subpolar gyre may be due to the curved coastline of the Alaskan peninsula-Aleutian Island chain, which causes the detachment of the Alaskan Stream from the northern coast (Thomson, 1972). The circulation of the tropical gyre is reduced in magnitude. This difference may be associated with the joint effect of baroclinicity and bottom relief. Knowing that the deep thermohaline circulation is strong in the tropics, we speculate that the effect of the thermohaline circulation near the bottom will be important.

Meridional overturn, zonally integrated stream function, for cases 1 through 4 is shown in Figure 2.3. In case 1, as in the work of Obata et al. (1996), the layered structure of the deep Pacific meridional circulation forms. There are two meridional circulation cells: (1) the northward flow of the Lower Circumpolar Water near the bottom and the southward return flow above it and (2) the northward flow at mid-depths and the southward flow near the sea surface. In case 2 the sea surface thermohaline forcing causes a shallow circulation cell with sinking in the north and upwelling in the south. Below this shallow cell the

layered structure in the deep Pacific meridional circulation seen in case 1 exists. In case 3 the imposed wind stress distorts the upper 1000 m circulation seen in case 1. The Ekman cells are dominant at the shallow depths, and the upper meridional circulation cell seen in case 1 is greatly intensified as a result of thermohaline circulation enhanced by wind forcing (chapter 3; Tsujino and Suginohara, 1998). Details of this circulation will be shown later. In case 4, when wind stress is imposed on case 2, the shallow circulation cell in case 2 seems to disappear. This event happens mainly because the intensified upper circulation cell found in case 3 rotates counterclockwise, tending to cancel out the clockwise circulation cell seen in case 2. A circle centered at about 30°N and 300 m is found in cases 3 and 4 in Figure 2.3. This is due to the strong upwelling at the western boundary as discussed below.

For a coarse resolution model like the present one it is inevitable to use a large horizontal diffusivity for stable numerical integration. Because the magnitude of vertical velocity on the inshore side of the western boundary layer is controlled by horizontal diffusivity (Warren, 1976; Masuda and Uehara, 1992), very strong upwelling/downwelling takes place at the western boundary in the coarse resolution model. In particular, the strong upwelling at the western boundary leads to broad offshore mid-depth downwelling, often referred to as the "Veronis effect" (Veronis, 1975). In the present model the upwelling between 30°N and 40°N for the shallow circulation cell in case 2 and strong upwelling at mid-depths in the northern half of the subtropical gyre for cases 3 and 4 are due to this effect (Figure 2.3). Such an upwelling or a downwelling at the western boundary, which dominates over that in the interior, occurs only at these latitudes.

Zonally averaged potential density field for cases 1 through 4 is shown in Figure 2.4. In case 1 the stratification is almost uniform throughout the ocean as a result of the constant reference density at the sea surface. In case 2 the imposed distribution of the sea surface reference density causes the weaker upper layer stratification at the higher latitudes. North of 45°N the vertical density gradient is weak at the upper 400 m depths, indicating that the convective adjustment reaches this depth there. In case 3 the meridionally uniform stratification in case 1 is distorted by the imposed wind stress: density surfaces are pushed down in the subtropical gyre (from 12°N to 45°N) and are sucked up in the subpolar gyre (north of 45°N). In case 4 the effects of the imposed wind stress appear similarly to those in case 3. In the subpolar gyre region the stratification at the upper 400 m depths is stronger

than that in case 2, indicating that the intense convective adjustment at the high latitudes seen in case 2 does not occur in case 4 and Ekman upwelling dominates (see also Figures 2.15 and 2.16). The distortion of isopycnals indicates that the depths to which the effect of the wind stress penetrates become deeper with increasing latitude. This finding supports the assertion of Reid and Arthur (1975).

To see details of the thermohaline circulation enhanced by wind forcing, the zonally integrated mass transport stream function and the zonally averaged density for the difference between cases 2 and 4 (case 4 minus case 2) are shown in Figure 2.5. The large-scale, very strong counterclockwise meridional circulation is formed at the thermocline depths. Note that the small cell centered at 30°N and 300m is due to the Veronis effect. The density becomes higher (the temperature becomes lower) in the upper layer of the subpolar gyre and in the surface layer of the equatorial region and becomes lower (the temperature becomes higher) in the upper layer near the southern boundary. The lower sea surface temperature in the subpolar gyre leads to a heat gain through the sea surface, and that in the equatorial region enhances the heat gain. These gains of heat through the sea surface in the subpolar gyre and the equatorial region are compensated by the loss of heat due to the higher temperature in the buffer region near the southern boundary. This causes a thermohaline circulation, a wind-enhanced thermohaline circulation (chapter 3; Tsujino and Suginohara, 1998), which connects the buffer region to the equatorial region and also to the subpolar gyre.

Now let us look at horizontal flow fields. Figures 2.6 through 2.8 show pressure fields in cases 1 through 4 at depths of 75 m, 355 m, and 585 m. For cases 3 and 4, lines of zero Sverdrup stream function are superimposed.

At 75m depth (Figure 2.6) the flow in the interior for case 1 is southwestward, which corresponds to the upper southward transport in Figure 2.3. This flow becomes the southward western boundary current at the low latitudes after hitting the western boundary. The flow in the interior in case 2 is nearly zonal. Because density at a depth of 75 m is strongly affected by the sea surface thermohaline forcing and the streamlines are approximately along the density contours, the flow is nearly zonal at this depth. The strong northward western boundary current is found south of 40°N, and it corresponds to the upper northward transport in Figure 2.3. Effects of the imposed wind stress are very strong at this shallow level, and the flows in cases 3 and 4 are similar. The three wind-driven gyres form in both cases.

The bifurcation latitude of the North Equatorial Current at the western boundary is one inferred from the Sverdrup stream function (12°N). A remarkable difference between cases 3 and 4 is found in the region south of 30°N. The flow in the interior in case 4 is eastward even south of 25°N and then becomes westward south of 15°N, while in case 3 the flow follows approximately the wind-driven circulation pattern. The westward flow in case 4 can be attributed to thermohaline effects: the flow north of 20°N in case 2 is eastward, and this flow is considered to appear in case 4. The appearance of thermohaline effects in the wind-driven circulation is more clearly seen in the meridional section of the zonal velocity, and it will be discussed later.

At 355 m depth (Figure 2.7) the southwestward flow seen at a depth of 75 m still exists in case 1, and it is recognized as the upper southward transport in Figure 2.3. The low-latitude southward western boundary current seen at 75 m also exists. In case 2 a broad southwestward flow is also found as in case 1. This flow corresponds to the southward return flow, which sinks from the sea surface at high latitudes, as seen in Figure 2.3. This flow begins at the northeastern corner of the basin, and it may correspond to the southward cross-gyre flow indicated by the salinity distribution of Reid (1973). After this southwestward flow reaches the western boundary, it becomes a relatively strong southward flow confined to the boundary region. In cases 3 and 4 the wind gyres are still strong. But in case 3 the subtropical gyre shrinks toward the west, and the flow in the eastern part of the subtropical gyre is weak. This feature is not found in case 4, where the subtropical gyre still dominates the midlatitude region, because the upper layer stratification is stronger in case 3; thus the wind-driven circulation is confined to the upper layer, especially in the eastern part, where higher-mode baroclinic Rossby waves from the eastern boundary do not dissipate. The southwestward flow of the northeastern origin seen in case 2 entirely disappears in case 4. A reason for this disappearance will be discussed in the next section. The bifurcation latitude of the North Equatorial Current at the western boundary shifts to the north by about 3° (15°N) for cases 3 and 4. The shift can be easily understood as the appearance of the thermohaline effects because there is a low-latitude southward western boundary current in cases 1 and 2.

At 585 m depth (Figure 2.8), in case 1, the southwestward flow found in the upper layer is confined to the northwest corner, and the northeastward flow dominates at the midlatitudes. This northeastward flow corresponds to the subsurface northward transport

in Figure 2.3. The low-latitude western boundary current flows northward and is weak. In case 2, though the southwestward flow seen at 355 m depth still dominates, its origin is not the water downwelled from the sea surface but the water upwelled from the deep layer. This corresponds to the upper southward transport found in the meridional circulation for case 1. The southward western boundary current is very strong. In cases 3 and 4 the subtropical and subpolar gyres are still clearly seen. But the subtropical gyre becomes weaker in the eastern and the southern part in comparison with that in the upper layer for both cases. This feature is more clearly seen in case 3 than in case 4. The tropical gyre becomes very weak in both cases. The bifurcation latitude of the North Equatorial Current at the western boundary is at about 16°N in case 4, but it is at about 12°N in case 3. This discrepancy is due to the thermohaline effects as seen at 355 m. Note that the subsurface southward flow exists for case 4 though the shallow meridional circulation cell found in case 2 disappears as a result of the occurrence of a wind-enhanced thermohaline circulation (chapter 3; Tsujino and Suginohara, 1998) as seen in Figure 2.3.

To see the detailed vertical structures, meridional sections of the zonal velocity along 180° in cases 1 through 4 are shown in Figure 2.9. The vertical structure of the thermohaline circulation is clearly seen in cases 1 and 2. In case 1, it is meridionally uniform in the upper layer as a result of the meridionally uniform stratification, while in case 2 it changes with latitude as a result of the weaker upper layer stratification at higher latitudes. Cases 3 and 4 have a similar flow pattern: the wind-driven pattern dominates the upper layer, and it penetrates deeper with increasing latitude. But at the upper 200 m depths from 15°N to 30°N there is a remarkable difference between cases 3 and 4. The westward flow in case 4 is far weaker than that in case 3, and even the eastward flow forms around 20°N. Comparison with the corresponding no wind-stress cases yields that this difference is attributable to thermohaline effects: the eastward flow at the sea surface seen in case 2 still exists around 20°N in case 4 because the strength of the wind-driven westward flow is comparable to that of the thermohaline eastward flow near the latitude of maximum wind stress curl (about 30°N). But in the northern half of the subtropical gyre in case 4, intensification of the eastward flow near the sea surface is not found. Thus it can be said that the thermohaline effect appears in the low-latitude upper layer where the wind-driven circulation is believed to be strong. Along the equator the subsurface eastward flow of the Equatorial Undercurrent is found in cases 3 and 4; this current is caused by wind forcing.

2.3.2 Thermohaline Effects on Upper Layer Circulation

In this subsection we look further into the effects of the sea surface thermohaline forcing by taking differences between cases that differ only in the sea surface thermohaline forcing: case 2 minus case 1 (hereafter difference 2-1), in which wind stress is absent, and case 4 minus case 3 (hereafter difference 4-3), in which wind stress is present.

Figure 2.10 shows the zonally integrated stream function and Figures 2.11 through 2.13 show the horizontal velocity fields at depths of 75 m, 355 m, and 585 m for the differences 2-1 and 4-3.

As found in Figure 2.10b for the difference 4-3, the upper meridional circulation cell as well as the Ekman circulation cell found in cases 3 and 4 (Figure 2.3) is almost removed. Figures 2.10a and 2.10b clearly demonstrate that effects of the sea surface thermohaline forcing are confined to the upper 1000 m depths. The clockwise circulation cell in the difference 2-1 corresponds to that seen in case 2 (Figure 2.3). Though the circulation in the difference 4-3 has some different characteristics, they have common features: downwelling at the high or middle latitudes and upwelling at the low latitudes, which compose the clockwise meridional circulation at the upper 1000 m depths.

At 75 m depth (Figure 2.11), in the difference 2-1, the western boundary current yields the surface northward transport seen in Figure 2.10a as in case 2 (Figure 2.6), while, in the difference 4-3, for the cases with wind forcing, various flows compose the northward transport: the northward current separates from the western boundary at 18°N, and it follows along the perimeter of the subtropical gyre and finally flows into the subpolar region, crossing the subtropical-subpolar gyre boundary in the eastern region. The strong eastward flow in the interior region around 20°N explains that the eastward flow seen for case 4 in Figures 2.6 and 2.9 is due to thermohaline effects. The southward western boundary current at the midlatitudes indicates that the western boundary current of the wind gyre for case 3 is stronger than that for case 4 near the sea surface, because the upper layer stratification is stronger in case 3 than in case 4, and thus the wind-driven gyre in case 3 is confined to the upper layer in comparison with that in case 4. The northward western boundary current at the high latitudes is explained in the same way.

At 355 m (Figure 2.12), in the difference 2-1, the subsurface southward flow with the westward component dominates the interior. After this flow hits the western boundary,

it forms the southward western boundary current flowing toward the equator. In the difference 4-3 the southwestward flow shifts to the perimeter of the subtropical gyre. This flow is stronger than that in the difference 2-1, and it crosses the subpolar-subtropical gyre boundary in the eastern region. But its continuation toward the equatorial region, i.e., the low-latitude western boundary current, is not clearly seen at this depth. The southward western boundary current at the midlatitudes seen at 75 m (Figure 2.11b) still exists, but the high-latitude northward western boundary current seen in Figure 2.11b disappears, and the southward flow takes over.

At 585 m (Figure 2.13), in the difference 2-1, the southwestward flow still dominates the interior. The low-latitude southward western boundary current seen at 355 m (Figure 2.12a) still exists, and it becomes stronger. In the difference 4-3, the southwestward flow in the midlatitude interior, which originates from the western high-latitude region and becomes the eastward jet along the subpolar-subtropical gyre boundary, crosses the subtropical-subpolar gyre boundary in the eastern region and follows the perimeter of the subtropical gyre. The low-latitude southward western boundary current, which corresponds to that in the difference 2-1, begins at 16°N. It is confirmed that the northward shift of the bifurcation latitude of the North Equatorial Current found for case 4 in Figure 2.8 is due to thermohaline effects. The midlatitude western boundary current becomes northward, and the high-latitude western boundary current becomes obviously southward, indicating that the wind gyre penetrates deeper in case 4 than in case 3 as a result of the weaker stratification at the high latitudes in case 4.

Depth, potential vorticity ($\rho^{-1} f \partial\rho/\partial z$), and horizontal velocity field on the isopycnal surface $\sigma_\theta = 26.6$ for case 4 are depicted in Figures 2.14a through 2.14c. The depth of this density surface is about 600 m in the middle- and low-latitude region. It is believed that the thermohaline effects dominate in the region where contour lines of potential vorticity emanate from the eastern boundary and terminate at the western boundary. This feature is found south of 18°N, which corresponds well with the observation (Talley, 1988). Thus the low-latitude circulation on $\sigma_\theta = 26.6$ is dominated by thermohaline circulation. Also, the horizontal velocity field resembles that of the difference 4-3 at 585 m (Figure 2.13b) in the low-latitude region. This finding confirms that the flow patterns explained as thermohaline circulation actually appear in the flow fields, even at shallow depths in the low-latitude region. Thus it is found that at the upper thermocline depths in the subtropical and

tropical regions the flows in the poleward and westward region are wind driven but those in the equatorward and eastward region are thermohaline.

It is well known that the intensity of thermohaline circulation depends upon the vertical diffusivity (e.g., Suginohara and Aoki, 1991). In the present model, when the vertical diffusion coefficient is taken to be larger, the thermohaline circulation increases in intensity, and hence its effect on the upper layer circulation becomes stronger, the cross-gyre flows being enhanced.

2.4 Discussion

In the present model, reproducibility of the salinity distribution is not good because of the coarse resolution. For example, the formation processes of NPIW at the subpolar-subtropical gyre boundary, such as the effects of mesoscale eddies (Talley et al., 1995; Yasuda, 1997), are not well represented, and thus the distribution of NPIW in the subtropical gyre is not expected to be well reproduced in the model.

Regions where convective adjustment occurs are shown for cases 2 and 4 in Figure 2.15. In case 2, there are roughly four regions where convective adjustment occurs: the high-latitude western boundary region, the high-latitude eastern boundary region, the midlatitude western boundary region, and the midlatitude interior region. The convection in the high-latitude eastern boundary region induces a salinity minimum layer in the subtropical gyre, which may correspond to Reid's minimum if it does not vanish in the presence of wind forcing. The midlatitude convection occurs because the high salinity water of low-latitude origin is transported northward by the western boundary current in the surface layer and is cooled in the interior region after it leaves the western boundary (see Figure 2.6). In case 4 there are three regions where convective adjustment occurs: the high-latitude western boundary region, the northwestern part of the subtropical gyre, and the equatorial regions. The high-latitude convection is also found in case 2. The midlatitude convection is associated with wind-driven circulation: the high-salinity water in the southern half of the subtropical gyre is brought to the northern part by the western boundary current and then is cooled to become denser than the water below. The convection in the high-latitude eastern region seen in case 2 does not exist in case 4, because the strong halocline, which prohibits convection, forms at the subsurface depths in the eastern part of the subpolar

gyre, which is discussed by using the salinity distributions below.

Here we look at the salinity distribution in case 4. Meridional sections of density and salinity along 155°E, 165°W, and 125°W for case 4 are shown in Figures 2.16a through 2.16c and Figures 2.17a through 2.17c, respectively.

In the 155°E section the salinity minimum centered approximately at $\sigma_\theta = 27.0$ is found. This minimum originates from the western North Pacific, including the Okhotsk Sea, where the sea surface density is the highest, $\sigma_\theta \sim 26.6$. This minimum may correspond to NPIW.

In the 165°W section, two salinity minima are found. Their centers are $\sigma_\theta = 25.7$ for the upper one and around $\sigma_\theta = 27.0$ for the lower one. The upper one originates from the western part of the subpolar-subtropical gyre boundary, where convective adjustment takes place. This may correspond to SSM of Tsuchiya (1982) and Yuan and Talley (1992), though the formation region in this model is located in the western region rather than in the eastern region. The lower one may be the continuation of that found in the 155°E section.

Along the 125°W section the single salinity minimum is found on about $\sigma_\theta = 26.0$. This may also correspond to SSM. Its origin is in the northwestern part of the subtropical gyre. Most of the water refreshed by convection is carried toward the east by the eastward jet along the subtropical-subpolar gyre boundary, and it begins to flow southward in the eastern part of the subtropical gyre.

Though the surface mixed layer in the high-latitude eastern region is observed to extend to about 150 m (Yuan and Talley, 1992), there is no such mixed layer in this model (Figure 2.16c). Instead the strong halocline that blocks convection is formed at the subsurface in the subpolar North Pacific (Figure 2.17c). A relatively saline water is brought to the high-latitude region by the wind-driven circulation in the subsurface layer, which causes the halocline. Thus the shallow meridional circulation seen in case 2 is not formed in case 4. In this model, part of SSM, the high-latitude origin in the eastern region seen in Reid's (1973) map, is not reproduced, possibly as a result of the lack of reproduction of the mixed layer.

2.5 Concluding Remarks

We have investigated the effects of the thermohaline forcing at the sea surface on the upper layer circulation of the North Pacific. The Pacific circulation north of 30°S is driven by wind forcing, thermohaline forcing at the sea surface, and Newtonian body forcing at the southern end of the model domain. Four cases with different sea surface forcing have been carried out: the constant sea surface reference density with and without wind stress and the observed sea surface reference density distribution with and without wind stress. The roles of each driving agent on the establishment of the North Pacific circulation are understood. Sea surface thermohaline forcing enhances the subsurface southward flow, which is the upper part of the layered deep Pacific meridional circulation. This flow suffers distortion but does not disappear even when wind forcing is imposed. It follows the eastern and the southern perimeter of the subtropical gyre, becoming the southward western boundary undercurrent at low latitudes. The cross-gyre southward western boundary undercurrent to the tropics indicated in the observed distribution of NPIW (e.g., Talley, 1993) is due to the thermohaline effect. Thus it is found that at the upper thermocline depths in the subtropical and tropical regions the flows in the poleward and westward region are wind driven, but those in the equatorward and eastward region are thermohaline. The behavior of AAIW in the low-latitude South Pacific and Atlantic may be accounted for in the same way as that of NPIW.

For the cases with wind stress the upper circulation cell in the layered deep Pacific meridional circulation is greatly intensified. This intensification leads to the disappearance of the shallow meridional circulation cell caused by sea surface thermohaline forcing, although the subsurface southward flow still exists. The intensification is due to a wind-enhanced thermohaline circulation, which connects the southern boundary to the subpolar gyre. A wind-enhanced thermohaline circulation (chapter 3; Tsujino and Suginohara, 1998) may play an important role in the general ocean circulation (Hasumi and Suginohara, 1998).

As Reid (1973) showed, the origin for part of SSM is north of the boundary between the subtropical and the subpolar gyre. It may be associated with the shallow thermohaline circulation of the high-latitude North Pacific origin. Since the vertical resolution of this model is not fine enough to precisely represent the mixed layer, in particular the convection in the high-latitude eastern North Pacific, Reid's minimum was not reproduced. Exact

reproduction of the mixed layer may be necessary to fully understand the formation and distribution of Reid's minimum.

Though the mechanisms for some flow patterns indicated by the observed tracer distributions are understood, tracer distributions themselves are not well reproduced in the present model. More precise representation of the water mass formation processes in the model will be needed. For SSM the mixed layer process, and for NPIW the mixing by mesoscale eddies in the mixed water region at the subtropical-subpolar gyre boundary, the effects of sea ice formation in the Okhotsk Sea and water exchange through the Kuril Islands should be subjects for a future investigation. Also, to understand the whole life of NPIW, the effects of the Indonesian throughflow need to be clarified.

Acknowledgments

We would like to thank Ryo Furue, Bill Holland, Toshio Suga, Mizuki Tsuchiya, Yasuhiro Yamanaka, and Ichiro Yasuda for pleasant discussions and helpful suggestions. All the figures are drawn with graphic routines in GFD-Dennou Library, developed by GFD-Dennou Club.

References

Bryan, K. (1984): Accelerating the convergence to equilibrium of ocean-climate models, *J. Phys. Oceanogr.*, **14**, 666–673.

Chen, L. G. and W. K. Dewar (1993): Intergyre communication in a three-layer model, *J. Phys. Oceanogr.*, **23**, 855–878.

Hasumi, H. and N. Suginohara (1998): Atlantic deep circulation controlled by heating in the Southern Ocean, *Geophys. Res. Lett.*, submitted.

Hellerman, S. and M. Rosenstein (1983): Normal monthly wind stress over the world ocean with error estimates, *J. Phys. Oceanogr.*, **13**, 1093–1104.

Levitus, S. (1982): *Climatological atlas of the world ocean*, U.S. Government Printing Office, Washington, D.C.

Luyten, J. R., J. Pedlosky and H. Stommel (1983): The ventilated thermocline, *J. Phys. Oceanogr.*, **13**, 292–309.

Masuda, A. and K. Uehara (1992): A reduced-gravity model of the abyssal circulation with Newtonian cooling and horizontal diffusion, *Deep Sea Res.*, **39**, 1453–1479.

McCreary, J. J. P. and P. Lu (1994): Interaction between the subtropical and equatorial ocean circulations: The subtropical cell, *J. Phys. Oceanogr.*, **24**, 466–497.

Obata, A., R. Furue, S. Aoki and N. Suginohara (1996): Modeling layered structure in deep Pacific circulation, *J. Geophys. Res.*, **101**, 3663–3674.

Reid, J. L. (1973): The shallow salinity minima of the Pacific Ocean, *Deep Sea Res.*, **20**, 51–68.

Reid, J. L. and R. S. Arthur (1975): Interpretation of maps of geopotential anomaly for the deep Pacific Ocean, *J. Mar. Res.*, **33 suppl.**, 37–52.

Suga, T. and L. D. Talley (1995): Antarctic intermediate water circulation in the tropical and subtropical South Atlantic, *J. Geophys. Res.*, **100**, 13,441–13,453.

Suginogara, N. and S. Aoki (1991): Buoyancy-driven circulation as horisontal convection on β-plane, *J. Mar. Res.*, **49**, 295–320.

Talley, L. D. (1985): Ventilation of the subtropical North Pacific: The shallow salinity minimum, *J. Phys. Oceanogr.*, **15**, 633–649.

Talley, L. D. (1988): Potential vorticity distribution in the North Pacific, *J. Phys. Oceanogr.*, **18**, 89–106.

Talley, L. D. (1993): Distribution and formation of North Pacific Intermediate Water., *J. Phys. Oceanogr.*, **23**, 517–537.

Talley, L., Y. Nagata, M. Fujimura, T. Iwao, T. Kono, D. Inagake, M. Hirai and K. Okuda (1995): North Pacific Intermediate Water in the Kuroshio/Oyashio mixed water region, *J. Phys. Oceanogr.*, **25**, 475–501.

Thomson, R. E. (1972): On the Alaskan Stream, *J. Phys. Oceanogr.*, **2**, 363–371.

Tsuchiya, M. (1982): On the Pacific upper-water circulation, *J. Mar. Res.*, **40 Suppl.**, 777–799.

Tsujino, H. and N. Suginohara (1998): Thermohaline circulation enhanced by wind forcing, *J. Phys. Oceanogr.*, in press.

Veronis, G. (1975): The role of models in tracer studies, in *Numerical Models of Ocean Studies*, National Academy of Science, 133–146.

Warren, B. A. (1976): Structure of deep western boundary currents, *Deep Sea Res.*, **23**, 129–142.

Yasuda, I. (1997): The origin of the North Pacific Intermediate Water, *J. Geophys. Res.*, **102**, 893–909.

Yasuda, I., K. Okuda and Y. Shimizu (1996): Distribution and modification of North Pacific Intermediate Water in the Kuroshio-Oyashio interfrontal zone, *J. Phys. Oceanogr.*, **26**, 448–465.

Yuan, X. and L. D. Talley (1992): Shallow salinity minima in the North Pacific, *J. Phys. Oceanogr.*, **22**, 1302–1316.

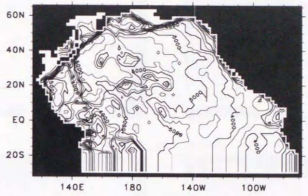

Figure 2.1: Model domain and bottom topography.

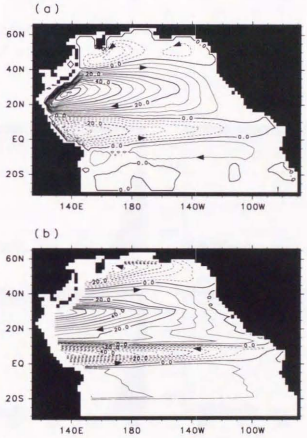

Figure 2.2: (a) Vertically integrated mass transport stream function for case 4, and (b) Sverdrup stream function calculated from Hellerman and Rosenstein's (1983) winter (February, March, and April) wind stress in Sv (1 Sv $= 10^6$ m^3 s^{-1}) units. Contour interval is 5 Sv.

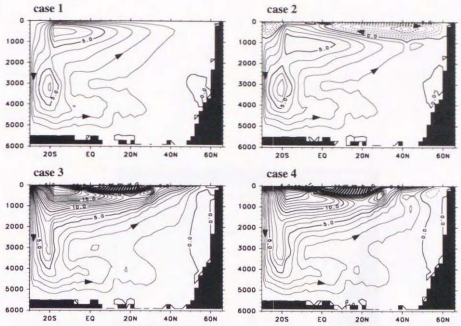

Figure 2.3: Zonally integrated mass transport stream functions for cases 1 through 4 in Sv units. Contour interval is 1 Sv.

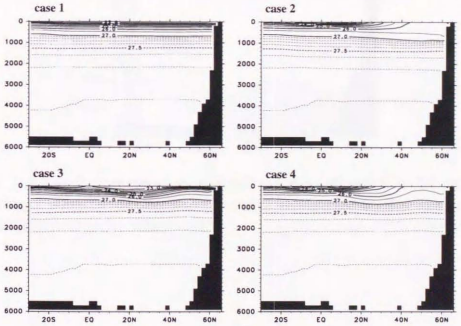

Figure 2.4: Zonally averaged potential density (σ_θ) field for cases 1 through 4. Contour interval is $0.5\sigma_\theta$. For density greater than 27.0 σ_θ, contour interval is 0.1 σ_θ.

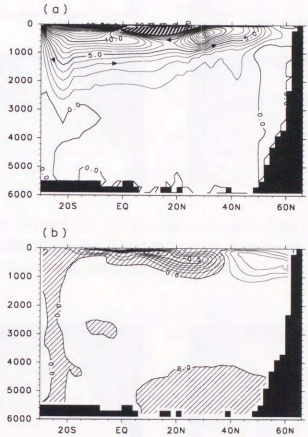

Figure 2.5: (a) Zonally integrated mass transport streamfunction in Sv units, and (b) zonally averaged potential density (σ_θ) for case 4 minus case 2. The shaded regions in Figure 2.5b indicate negative value.

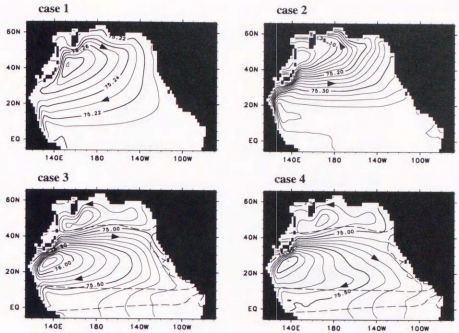

Figure 2.6: Pressure in decibars (db) at 75 m depth for cases 1 through 4. Contour interval is 0.01 db for case 1, 0.02 db for case 2, and 0.1 db for cases 3 and 4. For cases 3 and 4 the heavy dashed line represents zero Sverdrup stream function.

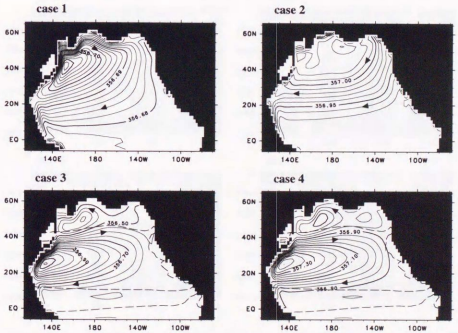

Figure 2.7: Same as Figure 2.6 except at 355 m depth. Contour interval is 0.002 db for case 1, 0.01 db for case 2, and 0.05 db for cases 3 and 4.

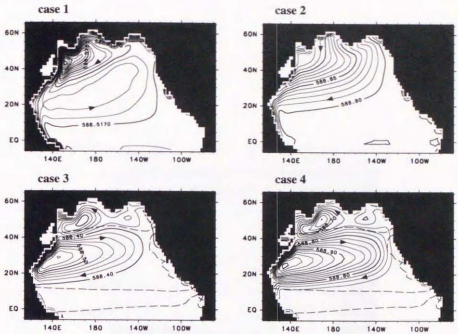

Figure 2.8: Same as Figure 2.6 except at 585 m depth. Contour interval is 0.0005 db for case 1, 0.01 db for case 2, and 0.02 db for cases 3 and 4.

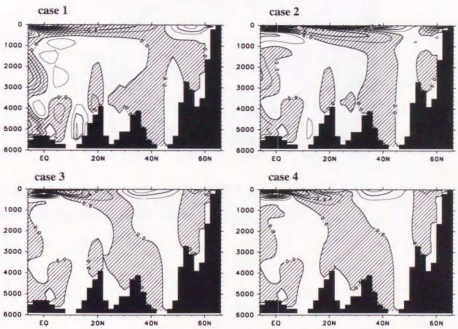

Figure 2.9: Meridional section of zonal velocity for cases 1 through 4 along 180°. Contour interval is 0.1 cm s^{-1} for case 1, 0.25 cm s^{-1} for case 2, and 2.0 cm s^{-1} for cases 3 and 4. The shaded regions indicate the westward flow.

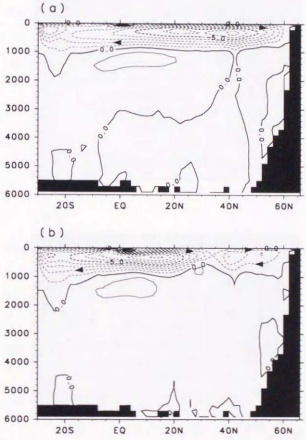

Figure 2.10: Zonally integrated mass transport stream functions for (a) case 2 minus case 1 and (b) case 4 minus case 3 in Sv units.

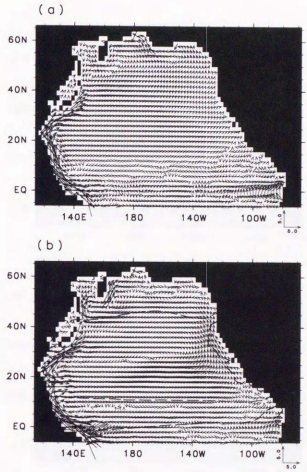

Figure 2.11: Horizontal velocity fields at 75 m for (a) case 2 minus case 1 and (b) case 4 minus case 3. The heavy dashed line in Figure 2.11b represents zero Sverdrup stream function. Unit vector is 5.0 cm s^{-1}.

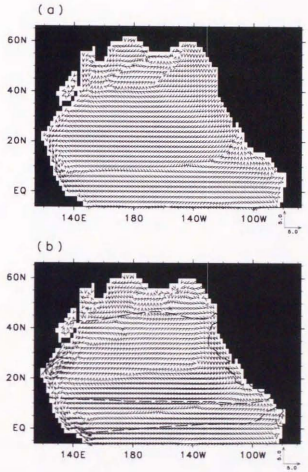

Figure 2.12: Same as Figure 2.11 but at 355 m depth.

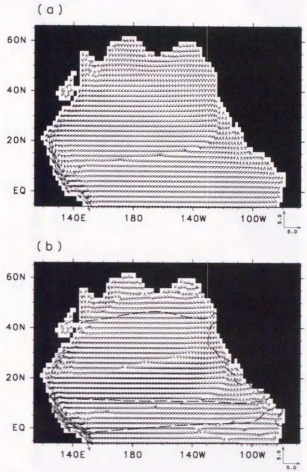

Figure 2.13: Same as Figure 2.11 but at 585 m depth.

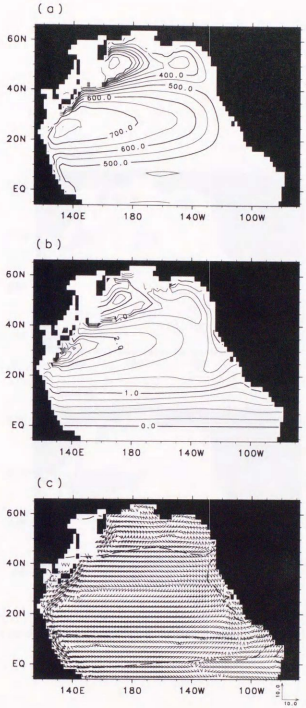

Figure 2.14: (a) Depth in meters, (b) potential vorticity ($\rho^{-1} f \partial\rho/\partial z$) in 10^{-12} cm^{-1} s^{-1}, and (c) horizontal velocity on the isopycnal surface, $\sigma_\theta = 26.6$, for case 4. Unit vector in Figure 2.14c is 10.0 cm s^{-1}.

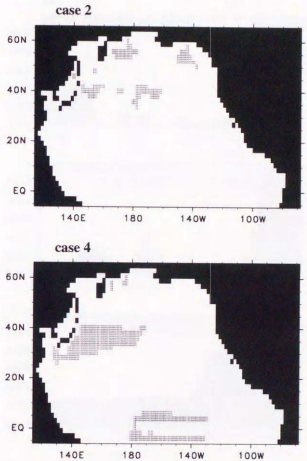

Figure 2.15: Areas where convective adjustment occurs for cases 2 and 4.

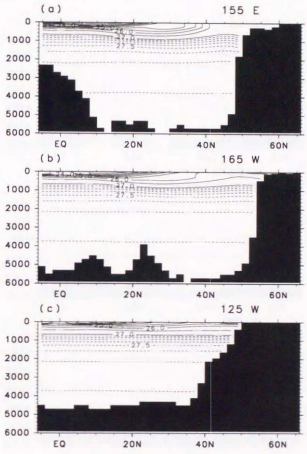

Figure 2.16: Meridional sections of potential density (σ_θ) for case 4 along (a) 155°E, (b) 165°W, and (c) 125°W.

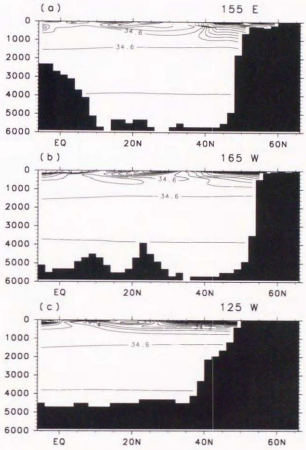

Figure 2.17: Same as Figure 2.16 except for salinity in psu. Contour interval is 0.1 psu.

Chapter 3

Thermohaline circulation enhanced by wind forcing

This chapter is from the paper by Tsujino and Suginohara which has been accepted for publication in Journal of Physical Oceanography.

Abstract

A thermohaline circulation enhanced by wind forcing is demonstrated in an idealized basin model, and a mechanism which provides a connection between wind forcing and a thermohaline circulation is clarified. A rectangular ocean which extends over the northern and southern hemispheres is driven by differential heating and wind stress at the sea surface. The differential heating is so distributed that the deep water is formed at the southern end of the model ocean. The wind stress is so distributed that there are three wind-driven gyres in the northern hemisphere, and it is not imposed in the southern hemisphere. Comparison is made between the cases with and without the wind stress. When the wind forcing is imposed, the basin-scale meridional circulation increases in intensity. This is due to the enhanced surface heating in the cyclonic wind-driven gyre with the Ekman upwelling and the accompanying enhanced surface cooling in the deep water formation region. In the cyclonic wind-driven gyre, the Ekman upwelling brings up the thermocline to the subsurface depths to enhance the surface heating and also the downward heat conduction from the sea surface to the deep layer, which leads to warming of the deep water. Thus, the enhanced surface heating in the cyclonic gyre is balanced with the enhanced surface cooling in the deep water formation region due to the warmed deep water. In this way, the wind forcing enhances a thermohaline circulation, a wind-enhanced thermohaline circulation, which connects the deep water formation region to the cyclonic wind-driven gyre with the Ekman upwelling.

3.1 Introduction

The thermohaline circulation is driven by the thermohaline forcing due to distribution of the heat and the fresh water flux through the sea surface. It is considered to take the form that the high density water formed in the concentrated region by convection upwells in the rest of the ocean to balance with downward conduction from the sea surface.

The wind forcing due to distribution of the wind stress over the ocean causes the Ekman upwelling/downwelling, and then it drives the wind-driven circulation. Since the Ekman *downwelling* pushes down the surface water and causes the circulation associated with the ventilated thermocline (Luyten et al., 1983), the thermohaline circulation is insulated from the thermohaline forcing in the subtropical gyre as argued by Samelson and Vallis (1997). On the other hand, the Ekman *upwelling* brings up the deep water to the subsurface depths and exposes it to the thermohaline forcing, which may cause a large heat gain in the region with the Ekman upwelling. Thus, the Ekman upwelling may force the conversion of dense deep water masses to the surface waters with much lower density. This implies an enhancement of the replacement rate of the deep water, and an amplification of the thermohaline circulation.

In fact, Toggweiler and Samuels (1995) pointed out that the formation of the North Atlantic Deep Water (NADW) and the outflow of NADW from the Atlantic are closely related to the wind stress over the Southern Ocean. They suggested the importance of the Ekman upwelling over the Southern Ocean in bringing up NADW to the sea surface.

In the North Pacific model (chapter 2; Tsujino and Suginohara, 1998), a large difference in meridional circulation at the subthermocline depths between cases with and without wind stress is found. That is, the upper circulation cell in the layered deep Pacific meridional circulation (Obata et al., 1996) is greatly intensified when the wind forcing is imposed. The strong circulation at the subthermocline depths is also found in the Pacific model of Ishizaki (1994) and in the world ocean circulation model of Nakata and Suginohara (1998). There seems to exist a large northward transport at mid-depths and a large southward transport near the sea surface for the meridional circulation in the Pacific, being caused by the wind forcing.

The purpose of this chapter is to demonstrate a thermohaline circulation enhanced by the wind forcing in an idealized basin model and to clarify a mechanism which provides

a connection between the wind forcing and the thermohaline circulation. We carry out numerical experiments for a single closed basin model with the deep water formation in the southern hemisphere and the wind forcing in the northern hemisphere. Three case-studies are made by changing wind-stress distribution to understand how the wind forcing affects the thermohaline circulation. First, the ocean is driven only by the thermohaline forcing. Next, the wind forcing is imposed and modification of the circulation is examined. The circulation driven by the wind stress with the reversed direction is also calculated to understand if results depend on a particular wind-stress distribution. Sensitivity to the vertical diffusivity and the meridional distribution of the thermohaline forcing is also investigated. Then, we will clarify a mechanism which provides a connection between the wind forcing and the thermohaline circulation. To accomplish this, we carry out some supplementary experiments, where a result for the case with wind stress is reproduced in a case without wind stress by parameterizing effects of the wind forcing.

This chapter is organized as follows. Section 3.2 describes the model. Results of calculations are presented in section 3.3 and the mechanism is discussed in section 3.4. Section 3.5 presents summary and discussion.

3.2 Experimental design

A rectangular ocean which extends over the northern and southern hemispheres as shown in Figure 3.1 is considered. The latitudinal width is 80° and the longitudinal width is 60°. The ocean has a flat bottom and is 4000 m deep.

The forcing agents are the buoyancy forcing and the wind forcing at the sea surface. The buoyancy forcing is made by restoring density to the reference value with the damping time of 60 days. The reference density, ρ_*, for the surface buoyancy forcing and the imposed zonal component of the wind stress are shown in Figures 3.2a and 3.2b. They are zonally uniform. The reference density is so distributed that the deep water is formed at the southern end of the model ocean. The wind stress is so distributed that there are three wind-driven gyres in the northern hemisphere, and it is not imposed in the southern hemisphere.

Three cases with different wind-stress distribution are carried out. First, the ocean is forced only by the sea-surface reference density distribution in Figure 3.2a (case I). Next, two types of wind-stress distribution are imposed on the case I. In one case the wind stress

is that shown in Figure 3.2b (case II). In the other case the direction of the wind in Figure 3.2b is reversed (case III). For the cases I and II, sensitivity to the vertical diffusivity is examined by taking the larger vertical diffusivity (cases I_{DIF} and II_{DIF}). Also sensitivity to the meridional distribution of the buoyancy forcing is examined by introducing the meridional gradient to the reference density (cases I_{DRD} and II_{DRD}).

Reproduction experiments are also carried out. Case I_{LED} is one of the cases where the vertical diffusivity is locally enhanced for the case I. The cases are listed in Table 3.1.

We use the Center for Climate System Research ocean general circulation model (CCSR-OGCM). The CCSR-OGCM is a multi-level model which solves the primitive equations under the hydrostatic, the Boussinesq, and the rigid-lid approximation. The finite differencing method is the same as that of Suginohara and Aoki (1991), where the weighted upcurrent scheme is adopted for the advection terms of density. Unstable stratification is removed by the convective adjustment: when potential density of a certain gridpoint is larger than that just below, potential density is homogenized downward from that gridpoint until unstable stratification is completely removed.

The horizontal resolution is $2^\circ \times 2^\circ$, and there are 32 levels in the vertical with high resolution near the sea surface (50 m) and decreased resolution toward the bottom (200 m).

We use the following values for the model parameters: $A_H = 8.0 \times 10^8\,\mathrm{cm^2\,s^{-1}}$, $A_V = 1.0\,\mathrm{cm^2\,s^{-1}}$, $K_H = 1.0 \times 10^7\,\mathrm{cm^2\,s^{-1}}$, and $K_V = 0.3\,\mathrm{cm^2\,s^{-1}}$, where A_H and A_V are the horizontal and the vertical viscosity coefficient, and K_H and K_V are the horizontal and the vertical diffusion coefficient.

The model equations are integrated for more than 6000 years to obtain a thermally and dynamically steady state, using Bryan's acceleration method (Bryan, 1984).

3.3 Results

The zonally integrated meridional transport stream function for the cases I through III is shown in Figure 3.3. In the case I without the wind stress, there forms the typical meridional circulation due to the buoyancy-driven circulation (e.g., Suginohara and Aoki, 1991). The deep water is formed at the southern end of the model ocean and the water slowly upwells in the rest of the ocean, which makes the large meridional circulation cell. When the wind

Table 3.1: List of experiments.

case	wind	vertical diffusivity	reference density in N. hemisphere
I	off	$0.3\,\mathrm{cm^2\,s^{-1}}$	constant (Figure 3.2a)
II	on	$0.3\,\mathrm{cm^2\,s^{-1}}$	constant (Figure 3.2a)
III	on (reversed)	$0.3\,\mathrm{cm^2\,s^{-1}}$	constant (Figure 3.2a)
$\mathrm{I_{DIF}}$	off	$1.0\,\mathrm{cm^2\,s^{-1}}$	constant (Figure 3.2a)
$\mathrm{II_{DIF}}$	on	$1.0\,\mathrm{cm^2\,s^{-1}}$	constant (Figure 3.2a)
$\mathrm{I_{DRD}}$	off	$0.3\,\mathrm{cm^2\,s^{-1}}$	distributed (Figure 3.10)
$\mathrm{II_{DRD}}$	on	$0.3\,\mathrm{cm^2\,s^{-1}}$	distributed (Figure 3.10)
$\mathrm{I_{LED}}$	off	locally enhanced*	constant (Figure 3.2a)

* see text

forcing is imposed, the Ekman cells are formed in the upper layer and the large meridional circulation cell is significantly intensified. In the region where the wind forcing induces the Ekman upwelling, i.e., in the cyclonic wind-driven gyre, the deep upwelling seems to be connected to the Ekman upwelling as seen for the cases II and III. Comparison between the cases II and III tells that the intensity of the large meridional circulation cell is almost the same in the two cases, though the circulation pattern in the northern hemisphere is slightly different. This indicates that the buoyancy-driven (thermohaline) circulation increases in intensity irrespective of the direction of the wind stress.

Zonally averaged density for the cases I through III is shown in Figure 3.4. The dense water formed at the southern end of the model ocean occupies the depths below the pycnocline. Density is almost meridionally uniform north of the deep water formation region in the case I. In the cases II and III, isopycnals are sucked up in the cyclonic wind-driven gyre with the Ekman upwelling and are pushed down in the anti-cyclonic gyre with the Ekman downwelling. Density in the deep layer becomes lower when the wind forcing is imposed (see also Figure 3.8).

Zonally averaged zonal velocity for the cases I through III is shown in Figure 3.5. In the northern hemisphere, strong flows associated with the wind-driven circulation are found in the cases II and III, and they are confined to the upper 1000 m depths. The three cases show the similar flow pattern in the deep layer except in the northern part of the northern hemisphere, where the wind-driven circulation dominates, i.e., the wind-driven circulation

penetrates into the deep layer. It is clearly seen that the flow in the southern hemisphere becomes stronger when the wind stress is imposed though the structure is almost the same as that of the case I. Thus, the intensity of the buoyancy-driven circulation is greatly affected by the wind forcing.

Figures 3.6a and 3.6b show the pressure field for the cases I through III at the depths of 75 m and 3100 m, respectively.

At 75 m (Figure 3.6a), in the case I, the anti-cyclonic gyre in the northern hemisphere is connected to the strong southward western boundary current in the southern hemisphere, which is the upper layer circulation pattern associated with the Stommel-Arons deep circulation for the Pacific (Suginohara and Aoki, 1991). When the wind forcing is imposed, three wind-driven gyres are formed in the northern hemisphere though the flow direction of the gyres is opposite between the cases II and III. The southward western boundary current as well as the interior eastward flow in the southern hemisphere is stronger for the cases II and III.

At 3100 m (Figure 3.6b), in the case I, the Stommel-Arons deep circulation pattern for the Pacific is formed, i.e., the northward deep western boundary current originating from the deep water formation region crosses the equator and feeds the cyclonic circulation in the northern hemisphere. When the wind forcing is imposed, the circulation in the southern hemisphere becomes stronger for both of the cases II and III. In the northern hemisphere, for the case II the cyclonic circulation becomes much stronger, and for the case III the cyclonic circulation becomes stronger but its center shifts to about 20°N. It is noted that as seen in Figure 3.5 the wind-driven circulation tends to penetrate into the deep layer in the northern part of the northern hemisphere.

Effects of the wind forcing on the buoyancy-driven circulation will be more clearly seen in the difference between the cases with and without the wind stress. Difference of the meridional transport stream function between the cases, (case II - case I) and (case III - case I), is shown in Figure 3.7. The basin-scale meridional circulation increases in intensity at all depths. The concentrated upwelling from the deep layer occurs in the region where the Ekman upwelling is taking place, and the upwelled deep water comes directly from the deep water formation region in the southern hemisphere without notable upwelling along the way. This suggests that the strength of the intensified circulation does not strongly depend upon the vertical diffusivity which is a crucial parameter for controlling the intensity

of the thermohaline circulation. The effect of the wind forcing on the meridional circulation is not confined to the upper layer. The wind forcing affects the intensity and structure of the large-scale buoyancy-driven (thermohaline) circulation.

Difference of the zonally averaged density between the cases, (case II - case I) and (case III - case I), is shown in Figure 3.8. When the wind forcing is imposed, density becomes lower in most of the ocean (most of the ocean is warmed) except near the sea surface in the region with the Ekman upwelling. There, isopycnals are sucked up and hence the density becomes higher compared with the case without the wind stress. Thus, the buoyancy (heat) budget through the sea surface may be greatly modified.

Sensitivity to the vertical diffusivity is examined. Differences between the cases $\mathrm{I_{DIF}}$ and $\mathrm{II_{DIF}}$, where the vertical diffusion coefficient is taken to be larger, $K_V = 1.0\,\mathrm{cm^2\,s^{-1}}$, are shown in Figure 3.9. The circulation in each case becomes stronger due to the larger diffusivity (not shown here). But, the differences of both the meridional transport stream function and the zonally averaged density are slightly smaller while their structures are not different than those in the small diffusivity case (compare with Figures 3.7a and 3.8a). The meridional circulation is less intensified with increasing the vertical diffusivity.

Sensitivity to the meridional distribution of the buoyancy forcing is also examined by introducing the meridional gradient to the reference density (cases $\mathrm{I_{DRD}}$ and $\mathrm{II_{DRD}}$). The reference density, the meridional transport stream function for the cases $\mathrm{I_{DRD}}$ and $\mathrm{II_{DRD}}$, and the difference, (case $\mathrm{II_{DRD}}$ - case $\mathrm{I_{DRD}}$), are shown in Figure 3.10. And the zonally averaged density for these cases and the difference are shown in Figure 3.11. The maximum value of the reference density at the northern end is set to be lower than that at the southern end (Figure 3.10). It is clearly seen also in this case that the wind forcing leads to the intensification of the basin-scale meridional overturning circulation and the warming of the deep water (compare with Figures 3.7a and 3.8a). A remarkable difference in meridional overturn from the cases I and II (Figure 3.3) is that there forms a local buoyancy-driven circulation at the subsurface depths in the northern hemisphere. It is noted that as seen in the difference in Figure 3.10 the concentrated deep upwelling is connected to the Ekman upwelling.

A case where the damping time for the restoring boundary condition for density at the sea surface is taken to be 30 days is also calculated in the case I and II. Almost the same results are obtained.

3.4 Mechanism

As shown in section 3.3, the effect of the wind forcing, even if it is remote from the deep water formation region, leads to the intensification of the global meridional overturning circulation, the circulation being less intensified with increasing the vertical diffusivity. Then, the problem may be how this circulation is established and whether it can be called a buoyancy-driven (thermohaline) circulation or not.

Difference between the calculated and the reference density, $\rho - \rho_*$, is depicted in Figure 3.12. This value is proportional to the buoyancy (heat) flux through the sea surface. When the wind forcing is imposed, the buoyancy gain (heating) becomes larger in the region with the Ekman upwelling in contrast to the region with the Ekman downwelling. This is because the *upwelled* water in the region with the Ekman upwelling causes the larger difference from the reference value. At the same time, the buoyancy loss (cooling) becomes larger at the southern end of the model ocean. This is due to the lower density (higher temperature) of the deep water (Figure 3.8), which causes the larger difference from the reference value in the deep water formation region. Thus, the buoyancy (heat) budget through the sea surface is greatly modified.

Vertical profiles of the terms in the density equation for the upper 500 m depths in the central subpolar gyre (29°E, 33°N) for the cases I and II are shown in Figure 3.13 (for the density equation, see Suginohara and Aoki, 1991). The vertical advection and the vertical diffusion term at the upper 100 m depths become much larger when the wind forcing is imposed. This feature is found everywhere in the subpolar gyre in contrast to the subtropical gyre where the horizontal and the vertical advection term dominate. The deep water brought up to the upper layer in the subpolar gyre with the Ekman upwelling is directly "heated" by conduction from the sea surface. Thus, the very active conversion from the deep water of high density to the surface water of low density takes place at the subsurface depths in the subpolar gyre, i.e., in the region with the Ekman upwelling.

Therefore, it is understood that in the region with the Ekman upwelling the wind forcing enhances the surface buoyancy flux and changes the density balance at the subsurface depths. It seems that the intensified global meridional overturning circulation seen for the cases with the wind stress is due to a buoyancy-driven (thermohaline) circulation enhanced by the wind forcing. If this is really a buoyancy-driven circulation, the intensified overturn-

ing circulation with the enhanced surface buoyancy fluxes should be reproduced for a case without wind stress by reasonably parameterizing the effect of the wind forcing in the density equation. As seen in Figure 3.13, the vertical diffusion becomes larger at the pycnocline (thermocline) depths in the subpolar gyre. So, for the case I, the vertical diffusion coefficient is significantly increased to $K_V = 3.0\,\mathrm{cm^2\,s^{-1}}$ in the domain between 30°N and 40°N and between 0 m and 420 m (case $\mathrm{I_{LED}}$). The meridional overturn and zonally integrated buoyancy flux for the case $\mathrm{I_{LED}}$ is shown in Figure 3.14. The intensified overturning circulation with the enhanced surface buoyancy fluxes in the case II is almost reproduced. In other words, the locally enhanced vertical diffusivity causes a buoyancy-driven circulation which connects the deep water formation region to the region with the enhanced vertical diffusivity. This feature is also reproduced for a case where the vertical advective flux of density due to the effect of the wind forcing is imposed on the density equation. Therefore, it is concluded that the intensified overturning circulation is due to a buoyancy-driven (thermohaline) circulation enhanced by the wind forcing. This thermohaline circulation can be called a "wind-enhanced thermohaline circulation". It should be remarked here that the intensified overturning circulation with the enhanced surface buoyancy fluxes is not reproduced even for a case where the surface reference density distribution is greatly modified.

Now, the intensification of the global meridional overturning circulation for the cases with the wind stress can be explained as follows. Starting with the steady state of the case I, let us impose the wind forcing on it. Isopycnals are sucked up in the cyclonic wind-driven gyre with the Ekman upwelling. There, the ocean gains more buoyancy (is heated) through the sea surface because the upwelled water causes the larger difference in density from the reference value, and also the deep water below the pycnocline gains more buoyancy by the enhanced downward conduction from the sea surface as seen in Figure 3.13. As a result, the deep ocean has the lower density (higher temperature) as seen in Figures 3.4 and 3.8. In a steady state, the excess buoyancy gain (heating) must be balanced by the excess buoyancy loss (cooling) somewhere. Considering the efficiency of buoyancy (heat) transfer by convection and conduction as is discussed in Suginohara and Aoki (1991), the compensatory buoyancy loss (cooling) can be done by convection in the very confined region. This occurs only in the deep water formation region at the southern end of the model ocean as shown in Figure 3.12. In fact, the deep water of lower

density (higher temperature) caused by the enhanced downward conduction in the cyclonic gyre leads to the larger difference from the reference density in the deep water formation region, which leads to the larger buoyancy loss and hence the larger production rate of the deep water. Thus, the wind-enhanced thermohaline circulation connecting the deep water formation region to the cyclonic wind-driven gyre is established.

Next, by using the mechanism understood above, we may explain why the circulation is less intensified with increasing the vertical diffusivity (Figure 3.9). With the larger vertical diffusivity, the stratification associated with the buoyancy-driven circulation without wind stress becomes diffuse. When the wind forcing is imposed on it, distortion of isopycnals caused by the wind stress penetrates deeper but its amplitude near the sea surface becomes smaller than in the small diffusivity case. The isopycnals coming to the sea surface have the lower density due to the diffuse stratification. Thus, the excess buoyancy gain through the sea surface in the cyclonic gyre is not so large as that in the small diffusivity case. Then, the intensity of the wind-enhanced buoyancy-driven (thermohaline) circulation in the large diffusivity case is not so strong as that in the small diffusivity case.

It is interesting to show the buoyancy flux through the sea surface for the cases $\mathrm{I}_{\mathrm{DRD}}$ and $\mathrm{II}_{\mathrm{DRD}}$ (Figure 3.15). As expected from the results in Figures 3.10 and 3.11, the buoyancy gain (heating) in the southern half of the subpolar gyre and the buoyancy loss (cooling) in the deep water formation region become larger when the wind forcing is imposed. The distribution of the buoyancy flux for the case $\mathrm{II}_{\mathrm{DRD}}$ is different than that for the case II (Figure 3.12). This is due to advection effects of the Ekman transport and the wind-driven western boundary current. These heating and cooling, except the enhanced heating in the southern half of the subpolar gyre, do not significantly affect the basin-scale thermohaline circulation: only the heating in the southern half of the subpolar gyre contributes to the warming of the deep water. Particularly, in the subtropical gyre, the deep water is insulated from the surface heating and cooling as argued by Samelson and Vallis (1997).

3.5 Summary and discussion

We have investigated the buoyancy-driven (thermohaline) circulation enhanced by the wind forcing. A rectangular ocean with flat bottom is driven by the buoyancy (thermohaline) and the wind forcing at the sea surface. The reference density for the buoyancy

forcing is constant except in the southern part of the southern hemisphere, where the deep water is formed. The wind stress is so distributed that there are three wind-driven gyres in the northern hemisphere, and it is not imposed in the southern hemisphere. Three cases have been carried out changing wind stress distribution: no wind stress, the wind stress, and the wind stress with the opposite direction. When the wind forcing is imposed, the basin-scale meridional circulation increases in intensity. This is due to the enhanced surface buoyancy gain (heating) in the cyclonic wind-driven gyre with the Ekman upwelling and the accompanying enhanced surface buoyancy loss (cooling) in the deep water formation region. In the cyclonic wind-driven gyre, the Ekman upwelling brings up the pycnocline (thermocline) near to the sea surface to enhance the surface buoyancy gain (heating) and also the downward conduction from the sea surface to deep layer. This results in the deep water of lower density (warming of the deep water), which leads to the enhanced buoyancy loss (cooling) in the deep water formation region. Thus, the enhanced surface buoyancy gain (heating) in the cyclonic gyre is balanced with the enhanced surface buoyancy loss (cooling) in the deep water formation region.

The vertical diffusion at the subsurface depths in the region with the Ekman upwelling dominates over that in the rest of the ocean. The intensified basin-scale overturning circulation with the enhanced surface buoyancy fluxes is reproduced for the case without the wind stress where the vertical diffusivity is locally enhanced, i.e., the vertical diffusivity is enhanced at the subsurface depths in the region corresponding to the cyclonic wind-driven gyre. Thus, it can be said that this intensified overturning circulation is due to the thermohaline circulation enhanced by the wind forcing, not being driven directly by the wind. This thermohaline circulation can be called the wind-enhanced thermohaline circulation, which connects the deep water formation region to the cyclonic wind-driven gyre. Its intensity becomes weaker with increasing the vertical diffusivity.

In the real ocean, the wind-enhanced thermohaline circulation is expected to connect a water-mass formation region to a region with the Ekman upwelling. As it is pointed out in Toggweiler and Samuels (1995) for NADW, the existing knowledge of the thermohaline circulation cannot account for the amount of the meridional overturning circulation. The wind-enhanced thermohaline circulation may complement this shortage. In fact, Hasumi and Suginohara (1998) clearly demonstrate that the wind-enhanced thermohaline circulation is found both in the Atlantic and the Pacific in their world ocean circulation

model with a high accuracy tracer advection scheme, UTOPIA/QUICKEST (Leonard et al., 1993), which enables them to adopt the observed small vertical diffusion coefficient, $K_V = 0.1\,\mathrm{cm^2 s^{-1}}$ (Ledwell et al., 1993).

Here, it is necessary to discuss on applicability of the present result to a coupled ocean-atmosphere system. It is naturally accepted that in an ocean only model the wind-induced upwelling causes a buoyancy gain as long as the surface boundary condition for the thermohaline forcing is in the form of restoring to the observed temperature and salinity (e.g., chapter 2; Tsujino and Suginohara, 1998). However, in the coupled system, this type of the surface boundary condition is suitable only for the surface heat flux but not for the surface fresh water flux. That is, precipitation and evaporation are not directly related to the wind-induced upwelling, though the upwelling leads to changes in the thermal environments at the sea surface. To evaluate properly the effect of the wind forcing on the thermohaline circulation, it is indispensable to use a coupled ocean-atmosphere model.

Acknowledgments

We would like to thank Shigeaki Aoki, Ryo Furue, and Hiroyasu Hasumi for pleasant discussions and helpful comments. All the figures are drawn with graphic routines in GFD-Dennou Library, developed by GFD-Dennou Club.

References

Bryan, K. (1984): Accelerating the convergence to equilibrium of Ocean-Climate models, *J. Phys. Oceanogr.*, **14**, 666–673.

Hasumi, H. and N. Suginohara (1998): Sensitivity of a global ocean general circulation model to tracer advection schemes, *J. Phys. Oceanogr.*, submitted.

Ishizaki, H. (1994): A simulation of the abyssal circulation in the North Pacific Ocean. Part I: Flow field and comparison with observations, *J. Phys. Oceanogr.*, **24**, 1921–1939.

Ledwell, J. R., A. J. Watson and C. L. Law (1993): Evidence for slow mixing across the pycnocline from an open-ocean tracer-release experiment, *Nature*, **364**, 701–703.

Leonard, B. P., M. K. MacVean and A. P. Lock (1993): Positivity-preserving numerical schemes for multidimensional advection, *NASA Tech. Memo. 106055*, **ICOMP-93-05**.

Luyten, J. R., J. Pedlosky and H. Stommel (1983): The ventilated thermocline, *J. Phys. Oceanogr.*, **13**, 292–309.

Nakata, M. and N. Suginohara (1998): Role of deep stratification in transporting deep water from the Atlantic to the Pacific, *J. Geophys. Res.*, 1067–1086.

Obata, A., R. Furue, S. Aoki and N. Suginohara (1996): Modeling layered structure in deep Pacific circulation, *J. Geophys. Res.*, **101**, 3663–3674.

Samelson, R. M. and G. K. Vallis (1997): Large-scale circulation with small diapycnal diffusion: The two-thermocline limit, *J. Mar. Res.*, **55**, 223–275.

Suginogara, N. and S. Aoki (1991): Buoyancy-driven circulation as horisontal convection on β-plane, *J. Mar. Res.*, **49**, 295–320.

Toggweiler, J. R. and B. Samuels (1995): Effect of Drake Passage on the global thermohaline circulation, *Deep Sea Res.*, **42**, 477–500.

Tsujino, H. and N. Suginohara (1998): Thermohaline effects on upper layer circulation of the North Pacific, *J. Geophys. Res.*, **103**, 18,665–18,679.

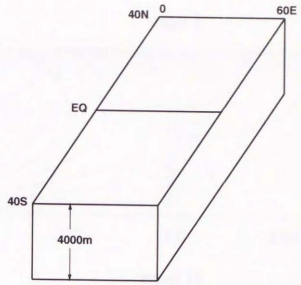

Figure 3.1: Schematic view of the model ocean.

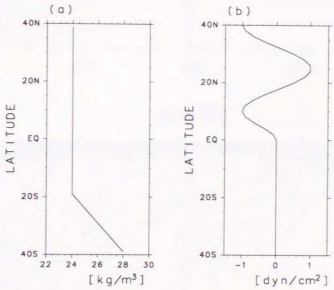

Figure 3.2: Meridional distribution of (a) the reference density and (b) the wind stress.

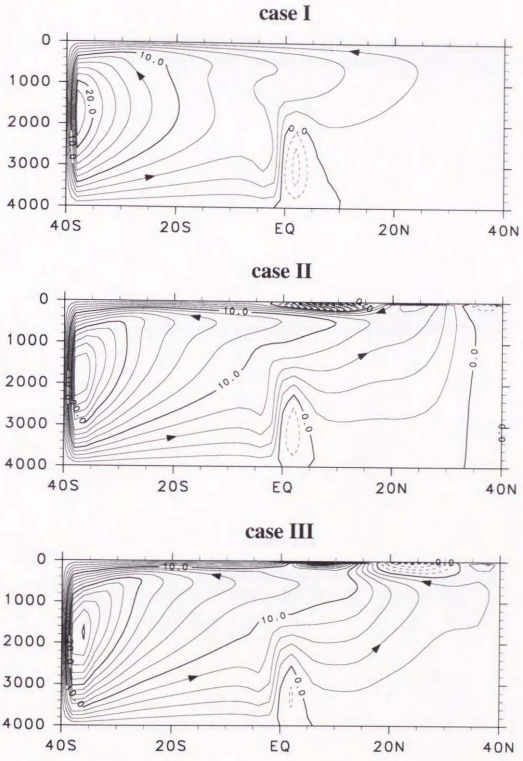

Figure 3.3: Zonally integrated mass transport stream function for the cases I through III in Sv ($= 10^6\,\mathrm{m}^3\,\mathrm{s}^{-1}$) units. Contour interval is 2 Sv.

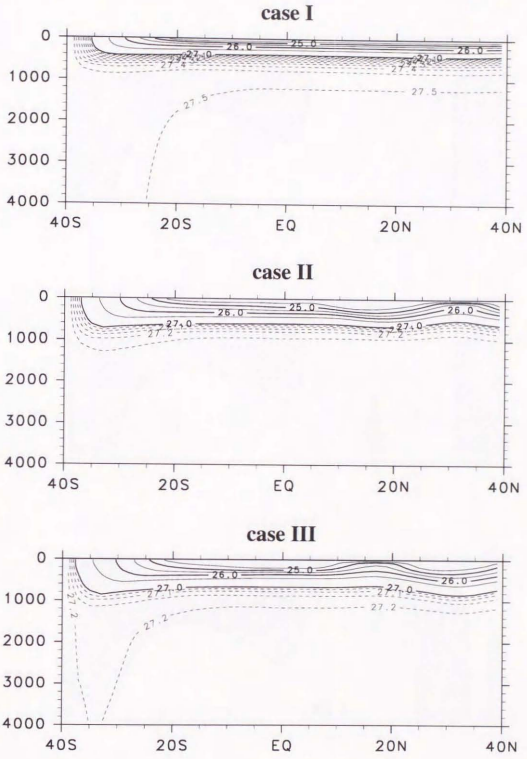

Figure 3.4: Zonally averaged potential density (σ_θ) for the cases I through III. Contour interval is 0.5 σ_θ. For density greater than 27.0 σ_θ, contour interval is 0.05 σ_θ.

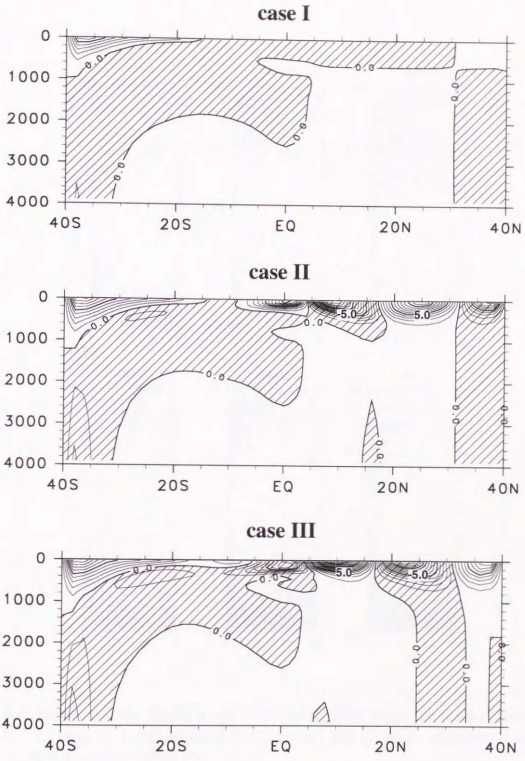

Figure 3.5: Zonally averaged zonal velocity for the cases I through III. Contour interval is 1.0 $\mathrm{cm\,s^{-1}}$. The shaded regions indicate the westward flow.

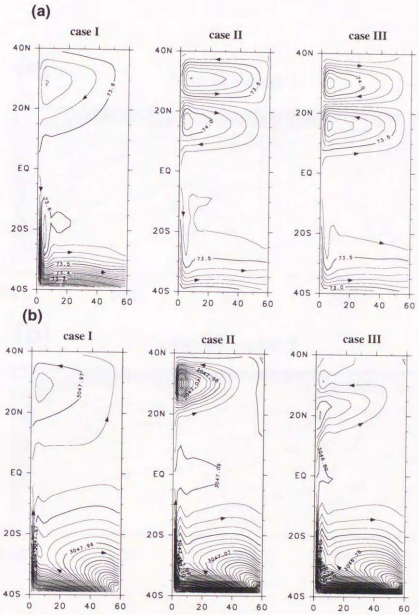

Figure 3.6: Pressure at the depths of (a) 75 m and (b) 3100 m for the cases I through III in db. In (a), contour interval is 0.02 db for the case I and 0.1 db for the cases II and III. In (b), contour interval is 0.0025 db.

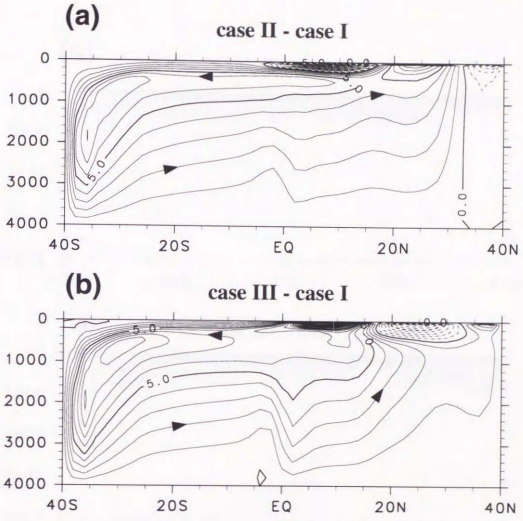

Figure 3.7: Difference of zonally integrated mass transport stream function, (a) (case II - case I) and (b) (case III - case I) in Sv units. Contour interval is 1 Sv.

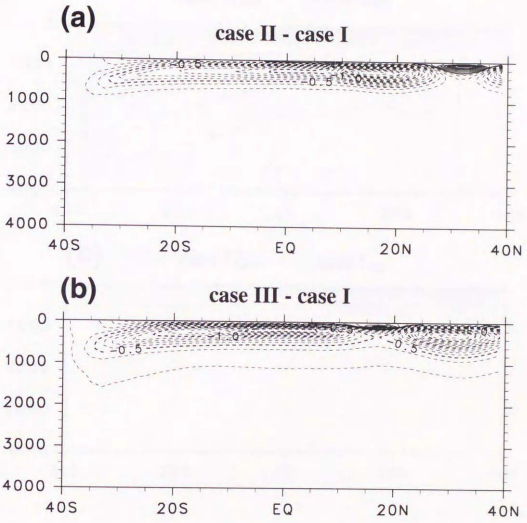

Figure 3.8: Difference of zonally averaged density, (a) (case II - case I) and (b) (case III - case I) in σ_θ. Contour interval is 0.1 σ_θ.

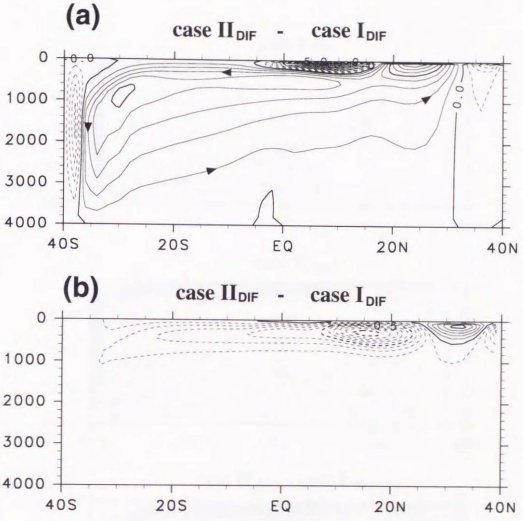

Figure 3.9: (a) Difference of zonally integrated mass transport stream function in Sv units and (b) that of zonally averaged density in σ_θ for (case $\mathrm{II}_{\mathrm{DIF}}$ - case $\mathrm{I}_{\mathrm{DIF}}$). Contour intervals are 1 Sv in (a) and 0.1 σ_θ in (b).

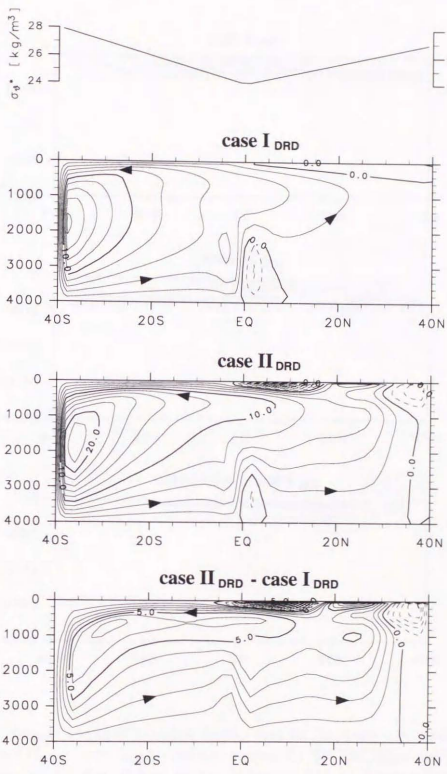

Figure 3.10: Reference density, zonally integrated mass transport stream function for the cases I_{DRD} and II_{DRD}, and difference, (case II_{DRD} - case I_{DRD}), in Sv units. Contour interval for the cases I_{DRD} and II_{DRD} is 2 Sv, and that for the difference is 1 Sv.

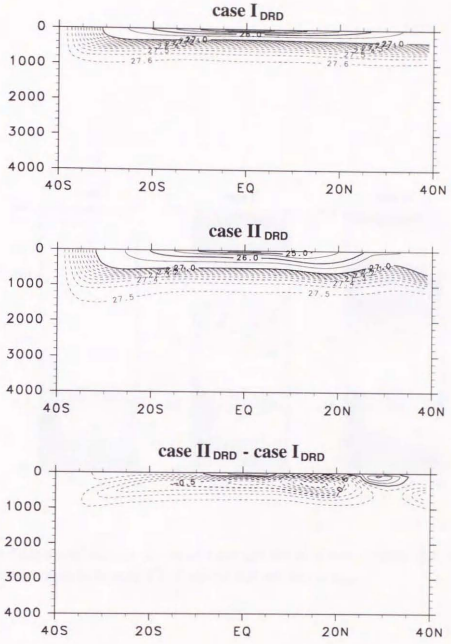

Figure 3.11: Zonally averaged potential density (σ_θ) for the cases I_{DRD} and II_{DRD}, and difference (case II_{DRD} - case I_{DRD}). Contour interval for the cases I_{DRD} and II_{DRD} is 0.5 σ_θ. For density greater than 27.0 σ_θ, contour interval is 0.05 σ_θ. Contour interval for the difference is 0.1 σ_θ.

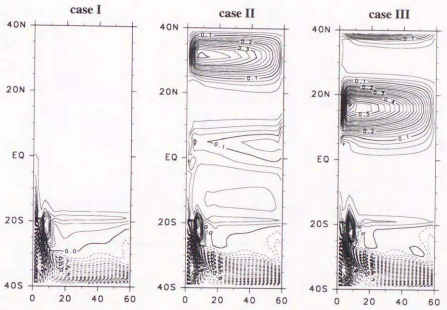

Figure 3.12: Difference between the calculated and the reference density at the sea surface, $(\rho - \rho_*)$, for the cases I through III. Contour interval is 0.025 σ_θ.

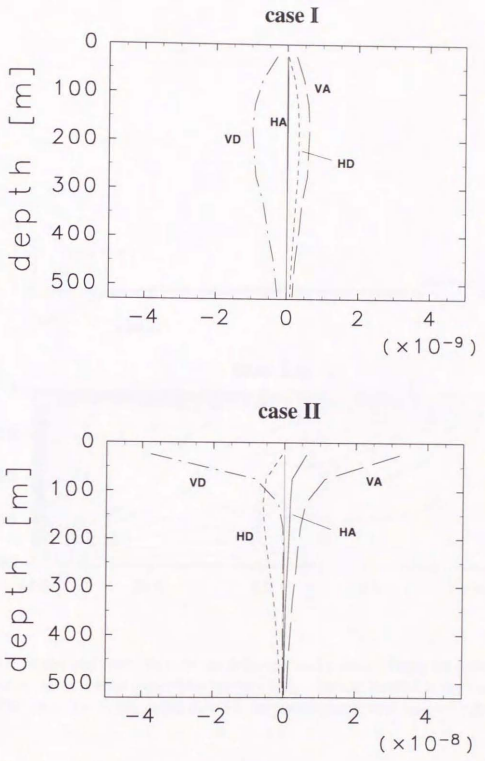

Figure 3.13: Vertical profiles of the terms in the density equation for the upper 500 m depths in the central subpolar gyre (29°E, 33°N) for the cases I and II. Note that the scale on the abscissa is different between the cases I and II. HA: horizontal advection, VA: vertical advection, VD: vertical diffusion, HD: horizontal diffusion. The unit of the abscissa is $\sigma_\theta \cdot s^{-1}$.

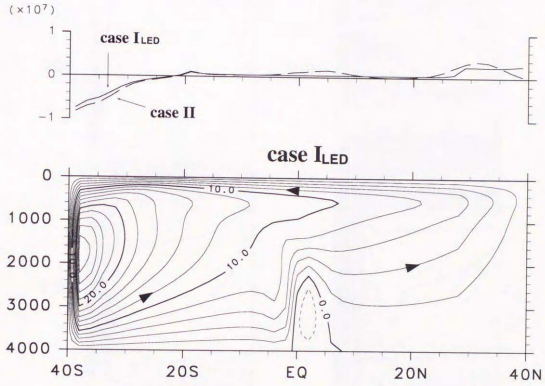

Figure 3.14: Meridional overturn in Sv units (lower) and zonally integrated surface buoyancy flux in $\sigma_\theta \cdot m^3 \cdot s^{-1}$ units (upper) for the case I_{LED}. Contour interval in the lower figure is 2 Sv. The dash line in the upper figure is for zonally integrated buoyancy flux in the case II.

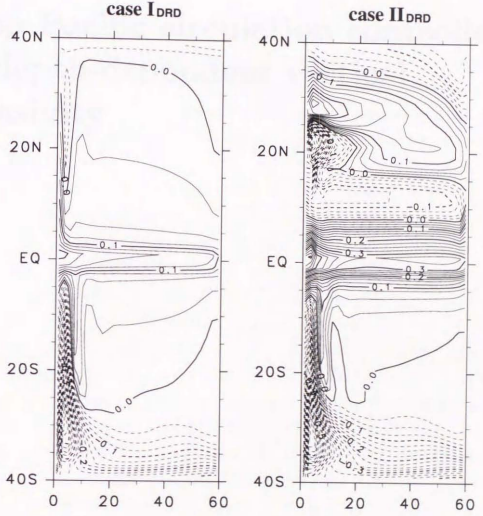

Figure 3.15: Difference between the calculated and the reference density at the sea surface, $(\rho - \rho_*)$, for the cases I_{DRD} and II_{DRD}. Contour interval is 0.025 σ_θ.

Chapter 4

Deep Pacific circulation controlled by depth-dependent vertical diffusivity

This chapter will be submitted to Journal of Physical Oceanography. Coauthors are H. Hasumi and N. Suginohara.

Abstract

Deep Pacific circulation is investigated by using an idealized two-basin model. Depth-dependent vertical diffusivity is employed to control the circulation. Vertical diffusivity estimated from observations, $0.1\,\mathrm{cm^2\,s^{-1}}$ and $3.0\,\mathrm{cm^2\,s^{-1}}$, is adopted for the upper layer and for the deep layer, respectively. Comparison is made among cases with different profiles of vertical diffusivity at mid-depths. When vertical diffusivity is set to increase progressively with depth beginning at the lower thermocline depths, the deep circulation is significantly intensified. This is due to enhanced heat exchange between the thermocline water and the deep water through the enhanced diffusion at the lower thermocline depths. The water below the thermocline is warmed and the water above the thermocline is cooled for the whole basin. The warmed deep water leads to enhanced deep water formation in the deep water formation region due to excess heat loss through the sea surface. The cooled upper-layer water leads to excess heat gain through the sea surface, balancing with the excess heat loss in the deep water formation region. The deep water upwelled to the lower thermocline depths does not further upwell to the sea surface due to the small upper-layer vertical diffusivity, but it flows back to the Southern Ocean, slowly upwelling at the thermocline depths. In this way, the meridional overturning with large transport forms below the lower thermocline in the Pacific. This circulation yields tracer distributions that are well compared with the observation.

When vertical diffusivity larger than $1.0\,\mathrm{cm^2\,s^{-1}}$ is taken in the deep layer, a set of alternating zonal jets, the stacked jets, along the equator is formed by the effect of vertical diffusion. The speed of the stacked jets is the greatest when vertical diffusivity increases with depth beginning at the lower thermocline depths. Thus, it is considered that the stacked jets can be explained as part of thermohaline circulation.

4.1 Introduction

Thermohaline circulation is driven by the distribution of the heat and the freshwater flux through the sea surface. It takes the form that high density water formed by convection in the very narrow region upwells in the rest of the ocean to balance with downward heat conduction from the sea surface (e.g., Suginohara and Aoki, 1991). Since there occurs no extensive dense water formation that leads to strong thermohaline circulation in the northern North Pacific, the deep and the bottom layer of the Pacific are filled with Circumpolar Deep Water (CDW) from the Southern Ocean, which is a mixture of North Atlantic Deep Water (NADW) formed in the northern North Atlantic and Antarctic Bottom Water (AABW) formed in the marginal seas of the Southern Ocean such as the Weddell Sea. CDW flows into the Pacific at the bottom, slowly upwells, and finally flows back to the Southern Ocean at mid-depths (Wunsch et al., 1983). For the northward transport of CDW in the Pacific, Wunsch et al. (1983) estimated 12 Sv in the South Pacific from *Scorpio* data by using an inverse method. Roemmich et al. (1991) and Wijffels et al. (1996) pointed out that about 10 Sv of CDW enters the North Pacific. Recently, Roemmich et al. (1996) and Rudnick (1997) obtained the northward abyssal transport of about 10 Sv through the Samoan Passage, supporting the above estimates. There is general agreement that about 10-20 Sv of CDW enters the South Pacific and about 10 Sv of it returns to the Southern Ocean at mid-depths. There is also agreement that about 10 Sv of CDW crosses the equator and it returns to the Southern Ocean as the silicate-rich deep water (Schmitz, 1995). This meridional circulation pattern in the deep Pacific is often referred to as the layered deep Pacific meridional circulation (e.g., Obata et al, 1996).

Numerical models have not reproduced the deep Pacific circulation with such a large amount of transport when vertically uniform vertical diffusivity between 0.3 and $0.5\,\mathrm{cm^2 s^{-1}}$ is used (e.g., Nakata and Suginohara, 1998; Hasumi and Suginohara, 1998a). In GFDL models where depth dependent vertical diffusivity with $0.3\,\mathrm{cm^2\,s^{-1}}$ in the upper layer and $1.3\,\mathrm{cm^2\,s^{-1}}$ in the bottom layer is used (Bryan and Lewis, 1979), inflow of CDW into the Pacific is not large, at most 9 Sv for the Indo-Pacific sector (e.g., England, 1993). Although there are some simulations where the realistic amount of transport is obtained, they all are artificial: Toggweiler and Samuels (1993) obtained an 8-Sv inflow of CDW into the North Pacific, but they artificially increased the formation rate of bottom water by adopting high

reference salinity (35.0 psu) in the Weddell Sea and the Ross Sea for the surface restoring boundary condition; Maier-Reimer et al. (1993) obtained a 10-Sv inflow of CDW into the North Pacific in Hamburg model, but most of it upwells to the sea surface near the equator because of large numerical diffusion arising from the up-current differencing scheme used in the tracer equations. The layered deep Pacific meridional circulation is formed in most of the models.

Care needs to be placed on that a transport estimated from observation is not the one obtained by zonal integration along constant depth surfaces but the one obtained by zonal integration along constant density surfaces. In the geostrophic transport calculation using zonal section data, a meridional transport of water mass for a certain density range is often obtained. Thus the zonal gradient of isopycnal surface is naturally taken into account. On the other hand, the meridional transport stream function usually used in presenting results of a numerical model is obtained by zonal integration of meridional velocity along constant depth surfaces. It is necessary to adopt the density coordinate as the vertical axis in calculating the meridional transport stream function to compare modeled transports with observed estimates (McIntosh and McDougall, 1996).

It is demonstrated that effects of wind forcing control intensity of the deep circulation in the Atlantic (Hasumi and Suginohara, 1998b) and the mid-depth circulation in the Pacific (chapter 3; Tsujino and Suginohara, 1998). However, the bottom circulation in the Atlantic and the deep circulation in the Pacific are not much affected by wind forcing (e.g., Hasumi and Suginohara, 1998b). They may be "classical" thermohaline circulation, where its intensity strongly depends on vertical diffusivity (e.g., Suginohara and Aoki, 1991).

What is known about vertical diffusivity? By microstructure measurements, Toole et al. (1994) and Polzin et al. (1997) obtained the diffusion coefficient of about $0.1\,\mathrm{cm^2 s^{-1}}$ for the interior ocean over smooth abyssal plains and the diffusion coefficient larger than $10.0\,\mathrm{cm^2 s^{-1}}$ on steeply sloping boundaries or over rough bottom. Small diapycnal diffusivity at the thermocline depths is also obtained by tracer-release experiments (e.g., Ledwell et al., 1993; Ledwell et al., 1998). Vertical diffusivity is estimated also from distributions of tracers such as temperature, salinity, and ^{14}C. Munk (1966), prescribing balance between vertical advection and vertical diffusion for tracers, obtained the value of $1.3\,\mathrm{cm^2 s^{-1}}$ from the lower thermocline to the deep layer. From heat budget calculation for bottom waters in semi-enclosed basins (Hogg et al., 1982), Roemmich et al. (1996) deduced vertical diffusivity of

500.0 cm^2s^{-1} near the bottom of the Samoan Passage, and Morris et al. (1997) obtained the basin-averaged vertical diffusivity of 3.0 cm^2s^{-1} for the bottom layer of the Brazil Basin.

In the present study, we intend to reproduce the deep Pacific circulation with the observed amount of transport. Considering that vertical diffusivity increases with depth, we clarify how depth-dependent vertical diffusivity controls the deep Pacific circulation. Vertical diffusivity is set to be 0.1 cm^2s^{-1} for the upper layer and 3.0 cm^2s^{-1} for the deep layer in accordance with the recent estimate from various observations. We examine how the deep circulation is affected by change in diffusivity at mid-depths.

There are a few studies where sensitivity to depth-dependent vertical diffusivity is investigated. Cummins et al. (1990) examined difference between a constant diffusivity case and a case with vertical diffusivity inversely proportional to Brunt-Väisälä frequency (Gargett, 1984). Cummins (1991) compared results among cases with different vertical profiles of vertical diffusivity below the thermocline. These experiments are performed for a rectangular basin in one hemisphere with a single deep water source, and change in density stratification and intensity of circulation are discussed: stratification is improved in the deep layer and thermohaline circulation is intensified, when vertical diffusivity is allowed to increase below the thermocline. However, its mechanism is not clarified.

Since the Pacific has no deep water source within it but has multiple deep water sources outside of it, situation for the Pacific may be different from a single basin model with a single deep water source. We carry out numerical experiments by using a two-basin model, where the two basins correspond to the Atlantic and the Pacific. With the use of zonal averages of the observed sea-surface temperature and sea-surface salinity in each basin for the surface restoring condition, the basic features of the global thermohaline circulation such as the deep water formation in the northern North Atlantic, the bottom water formation in the marginal seas of the Southern Ocean, and inflow of CDW into the Pacific can be reproduced (e.g., Nakata and Suginohara, 1998).

This chapter is organized as follows. Section 4.2 describes the model and the experimental design. Section 4.3 shows the results and clarifies the effects of depth-dependent vertical diffusivity on thermohaline circulation. Section 4.4 presents discussion and concluding remarks.

4.2 Model

We use the Center for Climate System Research ocean general circulation model (CCSR-OGCM). The CCSR-OGCM is a multilevel model that solves primitive equations under the hydrostatic, the Boussinesq, and the rigid-lid approximation. Except for advective tracer transport scheme, the numerical method is similar to that described by Bryan (1969). We use a high-accuracy advective tracer transport scheme, UTOPIA (Leonard et al., 1993). UTOPIA has the third order accuracy that has little numerical diffusion and dispersion, which enables us to adopt small vertical diffusivity such as $0.1\,\mathrm{cm^2 s^{-1}}$ for the upper layer. Performance of the CCSR-OGCM with UTOPIA is described by Hasumi and Suginohara (1998a).

Figure 4.1 illustrates the model ocean, which has two basins with sloping boundary. The depth in the interior is 5000 m. The larger basin corresponds to the Pacific. The zonal width is 90° in longitude, and the northern boundary lies at 60°N. The narrower basin extending further north to 72°N is the Atlantic, and the zonal width is 60°. The two basins are connected with a cyclic channel spanning the latitude band between 51°S and 63°S. The shallow channel with the depth of 2500 m connecting the eastern South Pacific and the western South Atlantic corresponds to the Drake Passage. The bottom topography near the boundary is smoothed not to induce numerical contamination such as extraordinary large vertical velocity, particularly at the Drake Passage sill. We call the regions south of the Atlantic and the Pacific as the Weddell Sea and the Ross Sea, respectively.

Isopycnal diffusion (Cox, 1987) is applied for the tracer equation, where the isopycnal eddy diffusion coefficient and the background horizontal eddy diffusion coefficient are chosen to be $1.0 \times 10^7\,\mathrm{cm^2 s^{-1}}$ and $1.0 \times 10^6\,\mathrm{cm^2 s^{-1}}$, respectively. The coefficients for the horizontal and the vertical eddy viscosity are $3.0 \times 10^9\,\mathrm{cm^2 s^{-1}}$ and $1.0\,\mathrm{cm^2 s^{-1}}$, respectively. The horizontal resolution is $3° \times 3°$ and there are 28 levels in the vertical with high resolution near the sea surface (50 m) and decreased resolution toward the bottom (250 m).

The zonal component of the imposed wind stress and the reference temperature and salinity for the surface restoring boundary condition is shown in Figure 4.2. The zonal wind stress is zonally uniform and has the same meridional dependence for both the Atlantic and the Pacific. The reference temperature and salinity are based on zonal averages of the observed winter sea-surface temperature (SST) and sea-surface salinity (SSS) of Levitus

Table 4.1: List of experiments

case	body forcing in the Weddell Sea	vertical diffusivity
I	on	Figure 4.3
II	on	Figure 4.3
III	on	Figure 4.3
IV	on	Figure 4.3
IIInbd	off	same as in the case III

(1982). Temperature and salinity at the sea surface are restored to the reference values with the damping time of 30 days.

Nakata and Suginohara (1998) pointed out that the presence of the marked density stratification in the circumpolar region well below the Drake Passage sill is essential for reproducing the realistic connection between the Atlantic and the Pacific. Following their suggestion, Newtonian body forcing is imposed at the southern end of the Weddell Sea at the depths between 4000 m and 5000 m. The body forcing is made by restoring temperature and salinity to the observed values in the abyssal layer of the Weddell Sea with the damping time of 10 days. The reference temperature and salinity are $T^* = -1.5°C$ and $S^* = 34.7$ psu, respectively. Owing to the short damping time, the body forcing is strong enough to overcome the intense diffusion in the deep layer caused by large diffusivity used in the present study.

We carry out five cases (Table 4.1). Vertical profiles of vertical diffusivity for the cases I through IV are shown in Figure 4.3. The case I is the control case where vertical diffusivity is constant $0.3\,\mathrm{cm^2\,s^{-1}}$. With the fixed vertical diffusivity, $0.1\,\mathrm{cm^2\,s^{-1}}$ for the upper layer and $3.0\,\mathrm{cm^2\,s^{-1}}$ for the deep layer taken from the observational estimates, cases with different profiles of vertical diffusivity at mid-depths are calculated. For the case II, vertical diffusivity begins to increase with depth around 1500 m. While for the case III, it begins to increase around 500 m: diffusivity at mid-depths is larger in the case III than in the case II. For the case IV, sensitivity to vertical diffusivity in the deep layer is examined, taking $1.0\,\mathrm{cm^2\,s^{-1}}$ for vertical diffusivity below 1000 m. The case IIInbd is to see effectiveness of the body forcing in the Weddell Sea for reproducing the connection between the Atlantic and the Pacific.

The model equations are integrated for more than 5000 years to obtain a thermally and dynamically steady state, using Bryan's acceleration method (Bryan 1984). Note that for the case III an average over the last 40 years is used for the analysis, as a small amplitude oscillation with 40-year cycle arises.

4.3 Results

4.3.1 Comparison among the cases with different profiles of vertical diffusivity

The zonally integrated meridional transport stream function in the Atlantic and the Pacific for the cases I through IV is shown in Figure 4.4. A two-basin model in the present study reproduces characteristics of meridional circulation in the world ocean such as the deep Atlantic circulation associated with NADW formation in the northern North Atlantic, the bottom Atlantic circulation associated with AABW formation in the Weddell Sea, and inflow of CDW into the deep Pacific. Comparison among the cases tells that the bottom Atlantic circulation and the deep Pacific circulation increase in intensity for the cases where vertical diffusivity of $3.0\,\mathrm{cm^2\,s^{-1}}$ is taken for the deep layer (case II and case III), while the deep Atlantic circulation shows a small difference. Transports of the bottom Atlantic circulation and the deep Pacific circulation for the case III are larger than those for the case II, which are well compared with the observational estimates. For the case III, in the Atlantic, the northward transport of AABW to the North Atlantic is about 5 Sv, which is slightly larger than the observational estimates of about 4 Sv (e.g., McCartney and Curry, 1993). In the Weddell Sea, the production rate of the bottom water amounts to 15 Sv, which is much larger than the observational estimates of about 5 Sv (e.g., Fahrbach et al., 1995). However, it should be noted that Broecker et al. (1998) recently estimated the production rate of 15 Sv by analyzing the distributions of chemical tracers. In the Pacific, the northward transport of CDW crossing the equator, 7 Sv, is comparable with the observation. But the layered deep meridional circulation seen in Obata et al. (1996) tends to disappear, the meridional circulation becoming a single cell with the northward inflow of CDW in the deep layer and the southward return flow to the Southern Ocean at mid-depths. Part of the return flow that reaches the Southern Ocean seems to join the upper-layer return flow of NADW in the Atlantic, and the rest flows back to the marginal

seas around the Antarctica. Thus, the bottom Atlantic circulation and the deep Pacific circulation are very sensitive to vertical diffusivity.

It is clearly seen that transports of both the bottom Atlantic circulation and the deep Pacific circulation are best reproduced for the case III with depth-dependent vertical diffusivity having about $1.0\,\mathrm{cm^2\,s^{-1}}$ at the depths around 1000 m and $3.0\,\mathrm{cm^2\,s^{-1}}$ in the deep layer. For the cases where vertical diffusivity has the large value at the depths around 1000 m (cases III and IV), the deep Atlantic circulation associated with NADW formation penetrates to the deeper depths and increases in intensity compared with the case where vertical diffusivity is not large there (case II). Intensity of the circulation is slightly weaker for the case III than for the case IV. The insignificant change in intensity indicates that intensity of the deep Atlantic circulation depends upon a factor other than vertical diffusivity. That is, as pointed out in Hasumi and Suginohara (1998b), the deep Atlantic circulation is enhanced by the heating caused by the Ekman upwelling in the Southern Ocean and its intensity does not strongly depend on vertical diffusivity. In the Pacific for each case except for the case I, most of the thermocline water upwelled from the deeper layer returns to the Southern Ocean without upwelling to the sea-surface. The upwelling to the sea surface occurs in the limited region with the Ekman upwelling such as the equator and the subpolar gyre in the North Pacific. This indicates that the mid-depth thermohaline circulation in the Pacific is enhanced by wind forcing as pointed out in Chapter 3 (Tsujino and Suginohara, 1998).

The zonally averaged density (σ_3) in the Atlantic and the Pacific for the cases I through IV is shown in Figure 4.5. The differences in meridional transport stream function among the cases can be explained by comparing the density fields. Note that in the Atlantic, $\sigma_3 = 41.5$ characterizes the lower limit of NADW. For the case III, because the isopycnal surface of $\sigma_3 = 41.5$ is pushed down due to the intense diffusion below 1000 m, NADW reaches deeper than for the case II, and the deep circulation associated with NADW formation occupies the depths as deep as 3000 m. The same thing happens for the case IV, confirming that the deep Atlantic circulation is affected by the enhanced mixing at mid-depths. In the Pacific, for the case II, density at the depths below 2500 m is considerably homogenized. Since vertical diffusivity is $3.0\,\mathrm{cm^2\,s^{-1}}$ at the depths below 2500 m, the homogeneous bottom water fills the depths below 2500 m without further mixing with the upper layer water with large heat content. Thus, for the case II, the deep Pacific circulation is not significantly

intensified because the bottom water is not warmed. For the case III, where vertical diffusivity has the large value at mid-depths, isopycnals are more crowded in the deep layer. Comparison between the Figure 4.3 and 4.5 tells that the lower thermocline lies at the depths where vertical diffusivity for the case III begins to increase. Considering that vertical diffusivity near the bottom is the same for the cases II and III, importance of mixing between the deep water and the lower thermocline water for reproducing the deep Pacific circulation is understood. CDW is warmed and upwelled, forming a strong single meridional circulation cell in the Pacific. Details of the effect of the enhanced vertical diffusivity at mid-depths will be discussed in the next subsection.

The zonally averaged zonal velocity in the Atlantic and the Pacific for the cases I through IV is shown in Figure 4.6. The structure of the zonal flow does not much differ among the cases. The speed of the Antarctic Circumpolar Current is greatest for the case III where the outflow of the bottom water from the Weddell Sea and the Ross Sea is the strongest. This is explained by the joint effect of baroclinicity and bottom relief, JEBAR (e.g., Mertz and White, 1992). Difference among the cases can also be seen at the equator: there exists a set of alternating zonal jets, "stacked jets", along the equator, whose speed in the deep layer increases with diffusivity in the deep layer and it is the greatest for the case III. The stacked jets in the deep layer at the equator is observed by Firing (1989) by direct current measurements. Suginohara and Fukasawa (1988), Suginohara and Aoki (1991), and Suginohara et al. (1991) pointed out that the stacked jets may be accounted for as part of thermohaline circulation, while Wang (1995) argued that the stacked jets reproduced by Suginohara and Aoki (1991) are an artifact due to excess diapycnal diffusion caused by large horizontal diffusivity.

Vertical profiles of the terms in the temperature equation at the depths below 1000 m in the equatorial Pacific for the case III are depicted in Figure 4.7. It is clearly shown that the vertical diffusion term plays an important role in the balance. When vertical diffusivity in the deep layer is $0.3\,\mathrm{cm^2\,s^{-1}}$, the vertical and lateral diffusion terms make the same contribution to the balance in the temperature equation. However, with increase of deep vertical diffusivity, even for the case IV, the vertical diffusion term comes to play an important role in the balance. Thus, large vertical diffusivity in the deep layer leads to formation of the stacked jets along the equator.

4.3.2 Role of enhanced diffusivity at mid-depths

In this subsection, to understand how the enhanced diffusivity at mid-depths intensifies the circulation, differences are taken between the case where vertical diffusivity has the large value at mid-depths and the case where vertical diffusivity is not large there: the case III minus the case II (hereafter difference III-II).

The zonally integrated mass transport stream function and zonally averaged density in σ_3 for the difference III-II are shown in Figure 4.8. In the Atlantic, the deep circulation associated with NADW formation is intensified, and the formation rate of bottom water in the Weddell Sea becomes larger. In the Pacific, there forms an enhanced meridional circulation below the thermocline with a northward inflow of CDW in the deep layer and a southward return flow at mid-depths, without upwelling to the sea surface within the Pacific. Note that the increased portion of NADW does not upwell in the Atlantic but flows out to the Southern Ocean below the depth of the Drake Passage sill: it flows into the Pacific as CDW, gains heat while slowly upwelling, and finally returns to the Atlantic at mid-depths. For density, the water below the lower thermocline is warmed and the water above the lower thermocline is cooled except for the northern North Atlantic and the southern end of the model ocean, where the deep and bottom waters are formed.

The above features are explained as follows. Owing to the enhanced vertical diffusivity at mid-depths, strong mixing between the deep and the lower thermocline water occurs, which leads to the warmer deep water and the colder thermocline water. In the upper layer, vertical diffusivity, though it is small, works so that the entire upper-layer water is cooled. The warmer deep water leads to the enhanced deep water formation due to excess heat loss in the deep water formation region. The colder upper-layer water leads to the enhanced heat gain through the sea surface to balance the excess heat loss in the deep water formation region. The enhanced vertical heat exchange at mid-depths causes the enhanced upwelling of the deep water to the lower thermocline. Since vertical diffusivity is small above the lower thermocline, the upwelled deep water does not further upwell to the sea surface, but it flows back to the deep water formation region, slowly upwelling at the thermocline depths. Thus, the intensified circulation below the lower thermocline in the Pacific is maintained.

Vertical profiles of the terms in the temperature equation at the depths below 600 m in the

central subtropical gyre of the North Pacific for the cases II and III are depicted in Figure 4.9. At the shallower depths above 600 m, all the terms, particularly the horizontal and the vertical advection term, become large because the wind-driven circulation is dominant. At the depths below 600 m, the balance between the vertical advection and the vertical diffusion holds for both cases. A marked difference can be found below 1000 m where the vertical advection and the vertical diffusion term become larger for the case III than the case II. The enhanced vertical diffusivity at mid-depths leads to the enhanced heat exchange in the deep layer as well as at mid-depths. Thus, the enhanced vertical diffusivity at mid-depths intensifies the thermohaline circulation below the thermocline depths.

4.3.3 Comparison with observation

In this subsection, we compare the results in the case III, where the amount of transport in the deep Pacific circulation is best reproduced, with the observation.

The meridional stream function, where zonal integration has been carried out along layers of constant potential density (σ_3), for the case III is shown in Figure 4.10. In the Pacific, about 11 Sv of CDW enters the South Pacific below $41.6\sigma_3$. About 4 Sv of it upwells in the South Pacific, and the rest, about 7 Sv, flows into the North Pacific. This feature resembles the circulation pattern for the deep Pacific of Schmitz (1995): 10-20 Sv of CDW enters the South Pacific and 10 Sv of it crosses the equator. The meridional stream function in Figure 4.4 yields the inflow of CDW into the South Pacific at the depths between 2500 and 5000 m. This depth range corresponds to the density range $\sigma_3 \geq 41.5$ (Figure 4.5). But, in the density range $41.5 < \sigma_3 < 41.6$, the flow is southward, which cannot be found in Figure 4.4 for the South Pacific. Thus, we should adopt the density coordinate as the vertical axis when model results are compared with observational estimates. This is important especially when large vertical diffusivity is taken for the deep layer: the strong vertical mixing causes intense water mass modification, leading to the large zonal gradient of isopycnals with respect to the surface of constant depth. For the bottom Atlantic circulation, 2 Sv of the bottom water upwells at the northern end of the basin. NADW formation there leads to the large horizontal gradient of isopycnals. This leads to the large diapycnal diffusive flux caused by horizontal diffusivity, resulting in strong heating of AABW by NADW. This explains why the inflow of AABW into the North Atlantic is slightly larger than the observational estimate of about 4 Sv (e.g., McCartney and Curry, 1993).

As seen in Figure 4.10, only a small amount of the deep water is upwelled across $\sigma_3 = 41.3$ in the South Atlantic, while the uniform upwelling across this isopycnal surface occurs in the entire Pacific. The upwelling across this isopycnal seen in the North Atlantic is largely due to the diapycnal diffusion at the western boundary caused by the horizontal diffusion (e.g., Böning et al. 1995). Balance between the vertical advection and the vertical diffusion in the temperature equation holds below the thermocline for the Pacific, while it does not for the Atlantic. This is because the deep circulation associated with NADW formation in the northern North Atlantic is a "wind-enhanced" thermohaline circulation (chapter 3: Tsujino and Suginohara, 1998) as demonstrated by Hasumi and Suginohara (1998b), where NADW upwells to the sea surface to gain heat only in the Southern Ocean with the Ekman upwelling. This Atlantic deep overturning pattern is different from a "classical" thermohaline circulation, where the vertical advection and the vertical diffusion are balanced for the whole basin. Part of NADW flows into the Pacific as CDW in the deep layer and upwells to the lower thermocline layer as the classical thermohaline circulation. Thus, characteristics of the deep thermohaline circulation in each basin strongly depend upon whether they are dominated by a wind-enhanced thermohaline circulation or not.

Horizontal velocity fields at the depth of 2875 m and 4875 m for the case III are shown in Figure 4.11. At 2875 m in the Pacific, there exists the southward flow continuing from the North Pacific to the Southern Ocean. It forms the western boundary current in the North Pacific and detaches from the western boundary at the low-latitude South Pacific. This southward flow corresponds to the lower part of the mid-depth southward flow that brings the silicate-rich deep water from the North Pacific to the South Pacific (Wunsch et al., 1983). As seen at 4875 m, the bottom water is formed mainly in the Weddell Sea, and it flows into the two basins. In the bottom layer, along the western boundary, the flow is northward and it connects to the relatively strong eastward jets along the equator, which forms the lowest part of the stacked jets.

Zonal sections of meridional velocity along 30°S, 18°S, and 6°S are shown in Figure 4.12. In the deep layer of the Pacific, there exists the strong northward western boundary current. This current corresponds to the inflow of CDW, which resembles Warren's (1973) observation in both depth and structure. Just above and to the east of the northward flow, there exists the southward flow. The core of the southward flow lies around the depth of 1000 m, which is shallower than Wunsch et al.'s (1983) estimate of around 1500 m.

Zonally averaged salinity in the Pacific is shown in Figure 4.13 along with that for climatology of Levitus (1982). The case III yields the salinity distribution in the Pacific that are well compared with the observed: the salinity minima at the intermediate depths in the northern and the southern hemisphere and the deep salinity maximum in the southern hemisphere. The deep salinity maximum in the southern hemisphere indicates that the high salinity water originating from NADW flows into the Pacific as CDW, i.e., the connection between the Atlantic and the Pacific deep water through the Southern Ocean is realistically established. Part of NADW that flows into the Southern Ocean from the Atlantic below the Drake Passage sill depth is well mixed with AABW by the enhanced vertical diffusion in the Southern Ocean to form a single deep water mass with high salinity signal on its top.

4.3.4 On the importance of body forcing

Here, effectiveness of the body forcing in the Weddell Sea for the present model is examined by comparing the cases with and without the body forcing. The meridional circulation, zonally averaged density, and zonally averaged zonal velocity in the Atlantic and the Pacific for the case IInbd is shown in Figure 4.14. It seems that there is almost no difference. However, horizontal velocity fields in Figure 4.15 show that the Pacific bottom water comes from the Ross Sea and that the southward flow in the Pacific at 2875 m becomes weaker. The deep Pacific is less stratified for the case IInbd (compare Figure 4.14 with Figure 4.5). This is because the AABW, which should be confined to the bottom layer, becomes a relatively thick homogeneous water in the deep layer. It is confirmed that as pointed out by Nakata and Suginohara (1998), the presence of the marked density stratification in the circumpolar region well below the Drake Passage sill is essential for reproducing the realistic connection between the Atlantic and the Pacific deep circulation.

4.4 Discussion and Concluding remarks

In this chapter, the deep Pacific circulation is investigated by using an idealized two-basin model. Depth-dependent vertical diffusivity is employed to control the circulation. Vertical diffusivity estimated from the observations is adopted, i.e., $0.1\,\mathrm{cm^2\,s^{-1}}$ for the upper layer and $3.0\,\mathrm{cm^2\,s^{-1}}$ for the deep layer. Comparison is made among the cases with

different profiles of vertical diffusivity at mid-depths, where the value of vertical diffusivity is not well known. When vertical diffusivity is set to increase with depth beginning at the lower thermocline depths, the deep Pacific circulation is significantly intensified with the enhanced deep and bottom water formation both in the northern North Atlantic and the Weddell Sea. This circulation yields tracer distributions that are well compared with the observation. Intensification of the deep Pacific circulation does not occur for the cases where vertical diffusivity is set to increase with depth beginning in the deep layer and where it is taken large at the lower thermocline depths but is not increase below that depths. Thus, it is found that to realistically reproduce the deep Pacific circulation, vertical diffusivity needs to be depth-dependent and it needs to take the large value of $1.0\,\mathrm{cm^2\,s^{-1}}$ at the lower thermocline depths and the larger value of $3.0\,\mathrm{cm^2\,s^{-1}}$ in the deep layer.

In the deep layer of the Southern Ocean, NADW and AABW are well mixed to form a single water mass of CDW due to the enhanced vertical diffusion in the deep layer. CDW that flows into the deep Pacific upwells to the lower thermocline layer due to the enhanced heat exchange with the thermocline water through the enhanced diffusion at the lower thermocline depths. The water below the thermocline is warmed and the upper-layer water is cooled for the whole basin. The warmed deep water leads to the enhanced deep water formation in the deep water formation region due to excess heat loss through the sea surface. The cooled upper layer water leads to excess heat gain through the sea surface, balancing with the excess heat loss in the deep water formation region. The upwelled deep water in the lower thermocline does not further upwell to the sea surface due to the small upper-layer vertical diffusivity, but it flows back to the Southern Ocean, slowly upwelling at the thermocline depths. In this way, the meridional overturning with larger transport forms below the lower thermocline in the Pacific. This mechanism carries over to the results of Cummins' (1991) experiments where a rectangular basin in one hemisphere with a single deep water source is considered. Thus, the deep Pacific circulation is considered to be the classical thermohaline circulation where its strength is strongly dependent on vertical diffusivity. This makes a remarkable contrast to the deep Atlantic circulation associated with NADW formation, which is the wind-enhanced thermohaline circulation (chapter 3; Tsujino and Suginohara, 1998) as demonstrated by Hasumi and Suginohara (1998b).

The production rate of AABW in the Weddell Sea is 15 Sv in the present model, which seems to conflict with the previous estimates of less than 5 Sv (e.g., Fahrbach et al., 1995).

Recently, however, Broecker et al. (1998) estimated the formation rate of 15 Sv using the distribution of chemical tracers. An exact estimation of the formation rate of AABW in the Weddell Sea and other marginal seas around the Antarctica should be a subject for future study.

Though horizontally uniform vertical diffusivity is adopted in the present study, the observations indicate that vertical diffusivity varies both vertically and horizontally (e.g., Toole et al., 1994; Polzin et al., 1997). Numerical experiments with enhanced vertical mixing near the coastal boundaries (Marotzke, 1997; Samelson, 1998) demonstrated that the stratification and the circulation in the interior for the boundary mixing case are significantly changed from those for the uniform mixing case while the intensity of thermohaline circulation is about the same when the zonal integral of vertical diffusivity is the same. Thus, knowledge of 3-D distribution of vertical diffusivity is necessary to reproduce the realistic circulation in OGCMs. Extensive observations and theoretical works that yield the detailed distribution of vertical diffusivity are strongly required.

When vertical diffusivity larger than $1.0\,\mathrm{cm^2\,s^{-1}}$ is taken in the deep layer, a set of alternating zonal jets, the stacked jets, along the equator, is formed by the effect of vertical diffusivity. The speed of the stacked jets is the greatest when vertical diffusivity increases progressively with depth beginning at the lower thermocline depths. Since recent observations show that vertical diffusivity in the bottom layer is large, it is considered that the stacked jets can be explained as part of thermohaline circulation. In future, a detailed comparison between the observation and the model is required. To achieve this, the model calculation should be made with higher horizontal resolution and real bottom topography.

Acknowledgment

We would like to thank Ryo Furue, Hideyuki Nakano, and Akira Oka for pleasant discussions and helpful comments. All the figures are drawn with graphic routines in GFD-Dennou Library, developed by GFD-Dennou Club.

References

Böning, C. W., W. R. Holland, F. O. Bryan, G. Danabasoglu and J. C. McWilliams (1995): An overlooked problem in model similations of the thermohaline circulation and heat transport in the Atlantic Ocean, *J. Clim.*, **8**, 515–523.

Broecker, W., S. L. Peacock, S. Walker, R. Weiss, E. Fahrbach, M. Schroeder, U. Mikolajewicz, C. Heinze, R. Key, T.-H. Peng and S. Rubin (1998): How much deep water is formed in the Southern Ocean?, *J. Geophys. Res.*, **103**, 15,833–15,843.

Bryan, K. (1969): A numerical method for the study of the circulation of the world ocean, *J. Comput. Phys.*, **4**, 347–376.

Bryan, K. (1984): Accelerating the convergence to equilibrium of Ocean-Climate models, *J. Phys. Oceanogr.*, **14**, 666–673.

Bryan, K. and L. Lewis (1979): A water mass model of the world ocean, *J. Geophys. Res.*, **84**, 2503–2517.

Cox, M. D. (1987): Isopycnal diffusion in a z-coordinate ocean model, *Ocean Modelling*, **74**, 1–5.

Cummins, P. F. (1991): The deep water stratification of ocean general circulation model, *Atmosphere-Ocean*, **29**, 563–575.

Cummins, P. F., G. Holloway and A. E. Gargett (1990): Sensitivity of the GFDL ocean general circulation model to a parameterization of vertical diffusion, *J. Phys. Oceanogr.*, **20**, 817–830.

England, M. (1993): Representing the global-scale water masses in ocean general circulation models, *J. Phys. Oceanogr.*, **23**, 1523–1552.

Fahrbach, E., G. Rohardt, N. Scheele, M. Schroeder, V. Strass and A. Wisotzki (1995): Formation and discharge of deep and bottom water in the northwestern Weddel Sea, *J. Mar. Res.*, **53**, 515–538.

Firing, E. (1989): Mean zonal currents below 1500 m near the Equator, 159°W, *J. Geophys. Res.*, **94**, 2023–2028.

Gargett, A. (1984): Vertical eddy diffusivity in the ocean interior, *J. Mar. Res.*, **42**, 359–393.

Hasumi, H. and N. Suginohara (1998a): Sensitivity of a global ocean general circulation model to tracer advection schemes, *J. Phys. Oceanogr.*, submitted.

Hasumi, H. and N. Suginohara (1998b): Atlantic deep circulation controlled by heating in the Southern Ocean, *Geophys. Res. Lett.*, submitted.

Hogg, N., P. Biscaye, W. Gardner and W. J. Schmitz (1982): On the transport and modification of Antarctic Bottom Water in the Vema Channel, *J. Mar. Res.*, **40 Suppl.**, 231–263.

Ledwell, J. R., A. J. Watson and C. S. Law (1993): Evidence for slow mixing across the pycnocline from an open-ocean tracer-release experiment, *Nature*, **364**, 701–703.

Ledwell, J. R., A. J. Watson and C. S. Law (1998): Mixing of a tracer in the pycnocline, *J. Geophys. Res.*, **103**, 21,499–21,529.

Leonard, B. P., M. K. MacVean and A. P. Lock (1993): Positivity-preserving numerical schemes for multidimensional advection, *NASA Tech. Memo. 106055*, **ICOMP-93-05**.

Levitus, S. (1982): *Climatological atlas of the world ocean*, U.S. Government Printing Office, Washington, D.C.

Maier-Reimer, E. M., U. Mikolajewicz and K. Hasselmann (1993): Mean circulation of the Hamburg LSG OGCM and its sensitivity to the thermohaline surface forcing, *J. Phys. Oceanogr.*, **23**, 731–757.

Marotzke, J. (1997): Boundary mixing and dynamics of three-demensional thermohaline circulation, *J. Phys. Ocanogr.*, **27**, 1713–1728.

McCartney, M. S. and R. A. Curry (1993): Transequatorial flow of Antarctic Bottom Water in the western Atlantic Ocean: Abyssal geostrophy at the Equator, *J. Phys. Oceanogr.*, **23**, 1264–1276.

McIntosh, P. C. and T. J. McDougall (1996): Isopycnal averaging and the residual mean circulation, *J. Phys. Oceanogr.*, **26**, 1655–1660.

Mertz, G. and D. G. Wright (1992): Interpretations of the JEBAR term, *J. Phys. Oceanogr.*, **22**, 301–305.

Morris, M., N. Hogg and W. B. Owens (1997): Diapycnal mixing estimated from advective budgets in the deep Brazil Basin, in *International WOCE Newsletter*, No. 28, 23–28.

Munk, W. H. (1966): Abyssal recipes, *Deep Sea Res.*, **13**, 707–730.

Nakata, M. and N. Suginohara (1998): Role of deep stratification in transporting deep water from the Atlantic to the Pacific, *J. Geophys. Res.*, 1067–1086.

Obata, A., R. Furue, S. Aoki and N. Suginohara (1996): Modeling layered structure in deep Pacific circulation, *J. Geophys. Res.*, **101**, 3663–3674.

Polzin, K. L., J. M. Toole, J. R. Ledwell and R. W. Schmitt (1997): Spatial variability of turbulent mixing in the abyssal ocean, *Science*, **276**, 93–96.

Roemmich, D., T. McCallister and J. Swift (1991): A transpacific hydrographic section along latitude 24°N: the distribution of properties in the subtropical gyre, *Deep Sea Res.*, **38 Supple. 1**, S1–S20.

Roemmich, D., S. Hautala and D. Rudnick (1996): Northward abyssal transport through the Samoan passage and adjacent regions, *J. Geophys. Res.*, **101**, 14,039–14,055.

Rudnick, D. L. (1997): Direct velocity measurements in the Samoan Passage, *J. Geophys. Res.*, **102**, 3293–3302.

Samelson, R. M. (1998): Large-scale circulation woth locally enhanced vertical mixing, *J. Phys. Oceanogr.*, **28**, 712–726.

Schmitz, W. J. (1995): On the interbasin-scale thermohaline circulation, *Rev. Geophys.*, **33**, 151–173.

Suginohara, N. and M. Fukasawa (1988): Set-up of deep circulation in multi-level numerical models, *J. Oceanogr. Soc. Japan*, **44**, 315–336.

Suginogara, N. and S. Aoki (1991): Buoyancy-driven circulation as horisontal convection on β-plane, *J. Mar. Res.*, **49**, 295–320.

Suginohara, N., S. Aoki and M. Fukasawa (1991): Comments on "On the importance of vertical resolution in certain ocean general circulation models", *J. Phys. Oceanogr.*, **21**, 1699–1701.

Toggweiler, J. R. and B. Samuels (1993): New radiocarbon constraints on the upwelling of abyssal water to the oceans's surface, in Heimann, M. ed., *The global carbon cycle*, NATO ASI Series, Springer-Verlag, Berlin, 333–366.

Toole, J. M., K. L. Polzin and R. W. Schmitt (1994): Estimates of diapycnal mixing in the abyssal ocean, *Science*, **264**, 1120–1123.

Tsujino, H. and N. Suginohara (1998): Thermohaline circulation enhanced by wind forcing, *J. Phys. Oceanogr.*, in press.

Wang, D. (1995): On thermally forced deep equatorial circulation in a GCM, *J. Phys. Oceanogr.*, **25**, 2155–2165.

Warren, B. A. (1973): Transpacific hydrographic sections at Lats. 43°S and 28°S: the SCORPIO Expedition - II. Deep water, *Deep Sea Res.*, **20**, 9–38.

Wijffels, S. E., J. M. Toole, H. L. Bryden, R. A. Fine, W. J. Jenkins and J. L. Bullister (1996): The water masses and circulation at 10°N in the Pacific, *Deep Sea Res.*, **43**, 501–544.

Wunsch, C., D. Hu and B. Grant (1983): Mass, Heat, Salt and nutrient Fluxes in the South Pacific Ocean, *J. Phys. Oceanogr.*, **13**, 725–753.

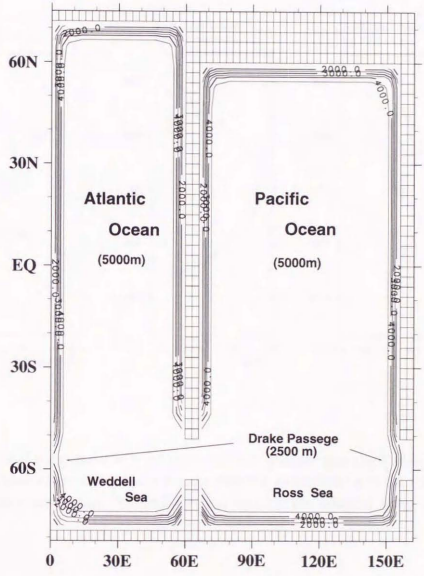

Figure 4.1: Geometry of the two-basin model.

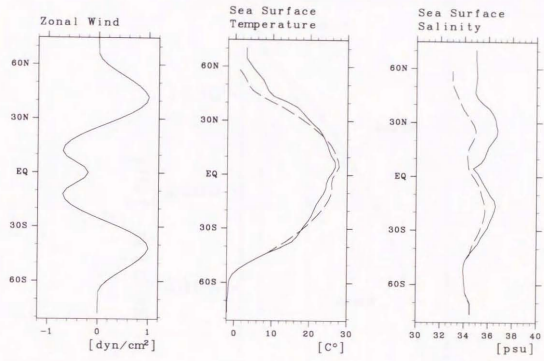

Figure 4.2: Zonal component of wind stress for the Atlantic and the Pacific, and reference sea-surface temperature and salinity for the Atlantic (solid line) and for the Pacific (dash line). Reference sea-surface temperature and salinity are adopted from Levitus' (1982) winter data.

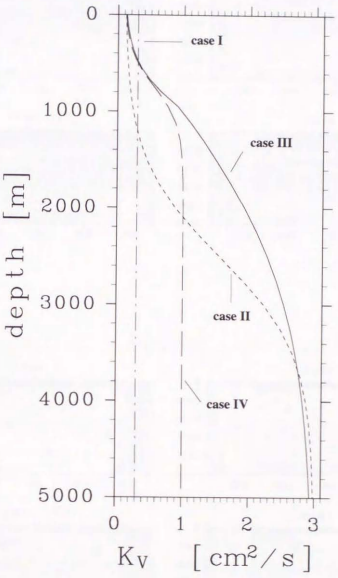

Figure 4.3: Vertical profile of vertical diffusivity for cases I through IV.

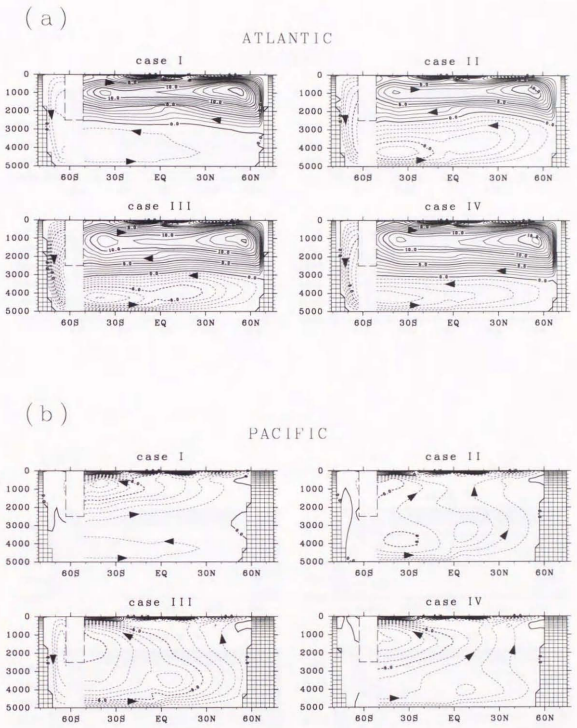

Figure 4.4: Zonally integrated mass transport stream function for (a) the Atlantic and (b) the Pacific in Sv units. Contour interval is 1 Sv.

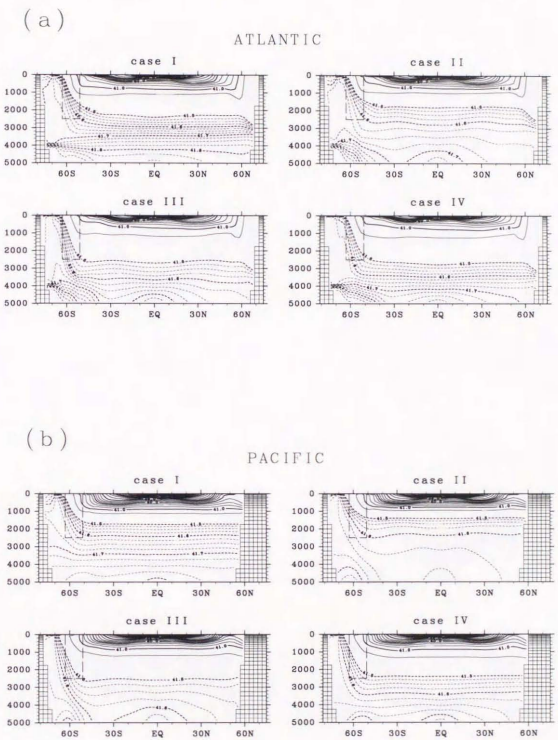

Figure 4.5: Zonally averaged potential density in σ_3 for (a) the Atlantic and (b) the Pacific. Contour interval is 0.25 σ_3. For density greater than 41.5 σ_3, contour interval is 0.025 σ_3.

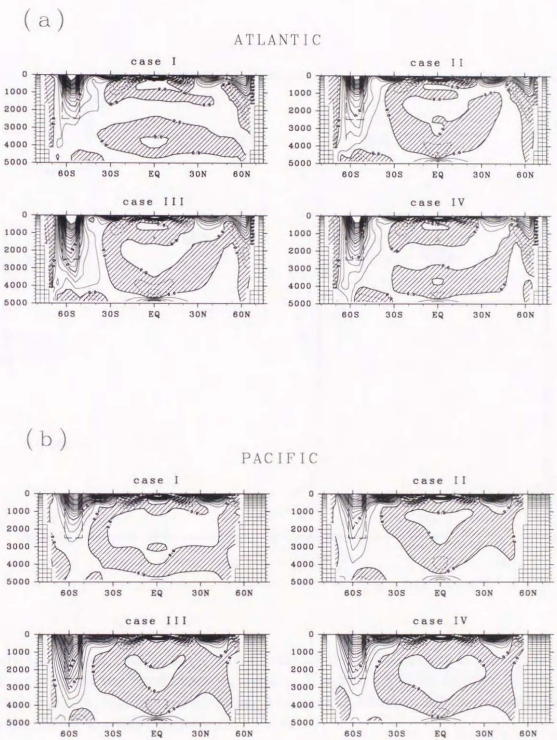

Figure 4.6: Zonally averaged zonal velocity for (a) the Atlantic and (b) the Pacific. Contour interval is 0.25 cm s^{-1}. The shaded regions indicate the westward flow.

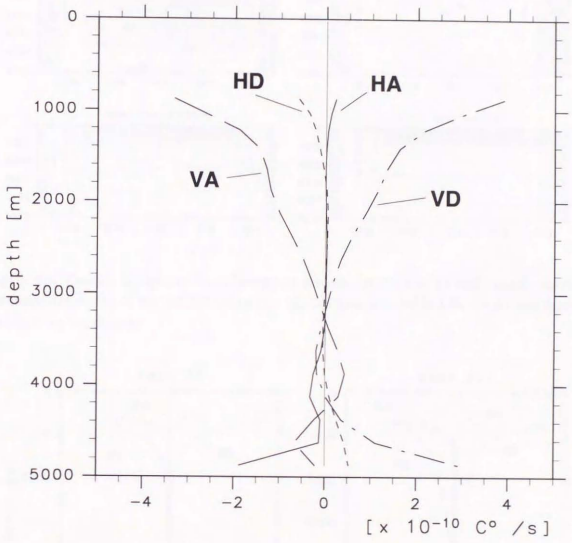

Figure 4.7: Vertical profiles of the terms in the temperature equation at the depths below 1000 m in the central Pacific near the Equator (118.5°E, 1.5°S) for the case III. HA: horizontal advection, VA: vertical advection, VD: vertical diffusion, HD: horizontal diffusion. The unit of the abscissa is degree $\cdot\, s^{-1}$.

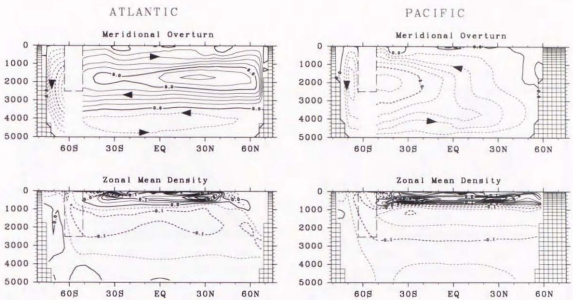

Figure 4.8: Zonally integrated mass transport stream function in Sv and zonally averaged potential density in σ_3 for the difference III - II. Contour interval is 1 Sv for stream function and 0.05 σ_3 for density.

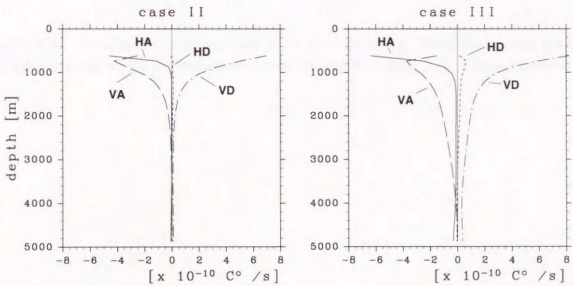

Figure 4.9: Vertical profiles of the terms in the temperature equation at the depths below 600 m in the central subtropical gyre of the North Pacific (118.5°E, 28.5°N) for the cases II and III. HA: horizontal advection, VA: vertical advection, VD: vertical diffusion, HD: horizontal diffusion. The unit of the abscissa is degree $\cdot\, s^{-1}$.

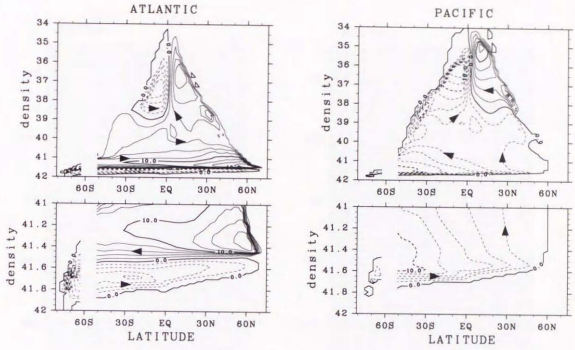

Figure 4.10: Meridional stream function in Sv for the case III. Zonal integration has been carried out along layers of constant potential density σ_3 (units: Sv). Contour interval is 2 Sv.

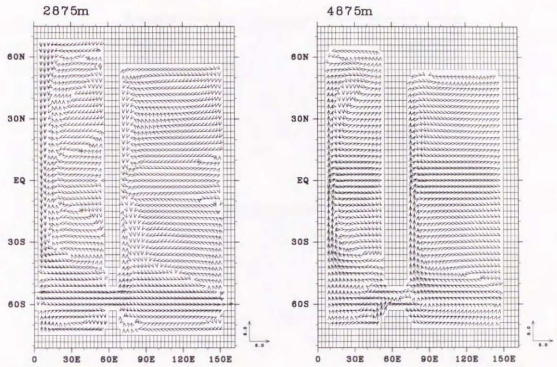

Figure 4.11: Horizontal velocity fields at 2875 m and at 4875 m for the case III.

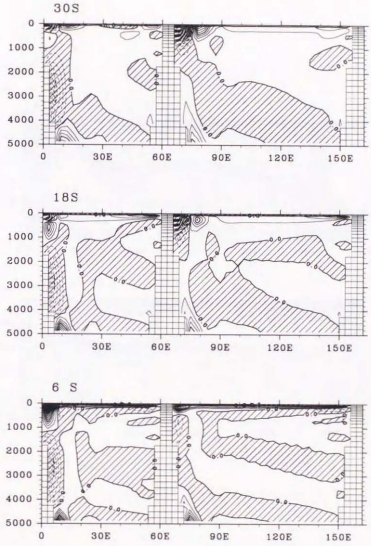

Figure 4.12: Zonal sections of meridional velocity for the case III along 30°S, (b) 18°S, and (c) 6°S. Contour interval is 0.5 cm s^{-1}. The shaded regions indicate the southward flow.

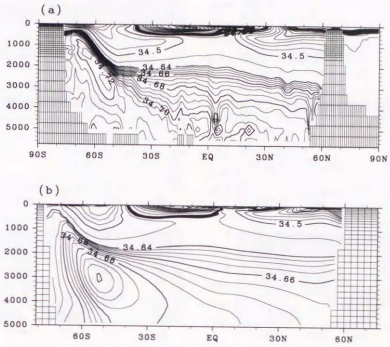

Figure 4.13: Zonally averaged salinity in the Pacific for (a) the climatology by Levitus (1982) and (b) the case III. Contour interval is 0.1 psu. For salinity between 34.64 psu and 34.7 psu, contour interval is 0.005 psu.

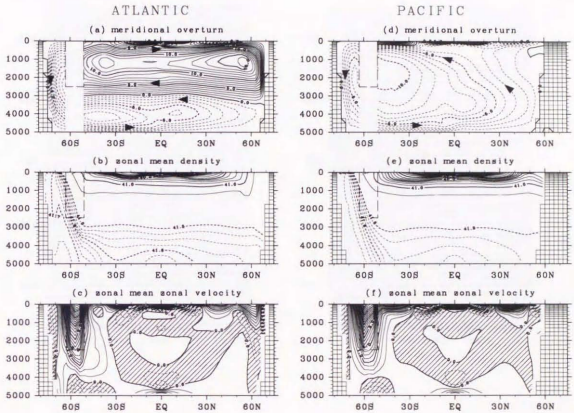

Figure 4.14: Results for the case IInbd. (a) Zonally integrated mass transport stream function in Sv, (b) zonally averaged density in σ_3, and (c) zonally averaged zonal velocity in $\mathrm{cm} \cdot \mathrm{s}^{-1}$ in the Atlantic. (D) through (f) are same as (a) through (c) except for the Pacific. Contour interval is 1 Sv for stream function, 0.25 σ_3 for density lighter than 41.5 σ_3, 0.025 σ_3 for density greater than than 41.5 σ_3, and 0.25 $\mathrm{cm} \cdot \mathrm{s}^{-1}$ for zonal velocity. The shaded regions for zonal velocity indicate the westward flow.

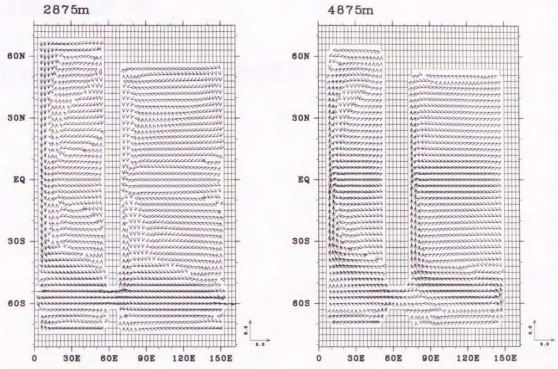

Figure 4.15: Horizontal velocity fields at 2875 m and at 4875 m for the case IInbd.

Chapter 5

General Conclusion

In the present thesis, thermohaline circulation in the Pacific Ocean has been investigated by carrying out process-oriented studies using numerical models. Problems in the upper layer, mid-depths, and deep layer in the Pacific are taken up, i.e., the way thermohaline circulation appears in the upper layer, effects of wind forcing on thermohaline circulation at mid-depths, and the role of depth-dependent vertical diffusivity in controlling the deep Pacific circulation.

First, thermohaline effects on the upper layer circulation of the North Pacific have been investigated. The Pacific circulation north of 30°S is driven by wind forcing, thermohaline forcing at the sea surface, and Newtonian body forcing at the southern end of the model domain. Four cases with different sea surface forcing are carried out: the constant sea surface reference density with and without wind stress and the observed sea surface reference density distribution with and without wind stress. By comparing the cases, the roles of each driving agent on the establishment of the North Pacific circulation are understood. The thermohaline forcing at the sea surface enhances the subsurface southward flow, which is the upper part of the layered deep Pacific meridional circulation. This flow suffers distortion but does not disappear, even when wind forcing is imposed. It follows the eastern and the southern perimeter of the subtropical gyre, becoming the southward western boundary undercurrent at low latitudes. The cross-gyre southward western boundary undercurrent to the tropics indicated in the observed distribution of North Pacific Intermediate Water (NPIW) (e.g., Talley, 1993) is due to the thermohaline effect. Thus it is found that at the upper thermocline depths in the subtropical and tropical regions the flows in the poleward and westward region are wind driven, but those in the equatorward and eastward region are thermohaline. The behavior of Antarctic Intermediate Water (AAIW) in the low-latitude South Pacific and Atlantic may be accounted for in the same way as that of NPIW.

Secondly, to clarify effects of wind forcing on thermohaline circulation at mid-depths, a mechanism which provides a connection between wind forcing and thermohaline circulation has been explored. A rectangular ocean which extends over the northern and southern hemispheres is driven by differential heating and wind stress at the sea surface. The differential heating is so distributed that the deep water is formed at the southern end of the model ocean. The wind stress is so distributed that there are three wind-driven gyres in the northern hemisphere, and it is not imposed in the southern hemisphere. Comparison is made between the cases with and without the wind stress. When the wind forcing

is imposed, the basin-scale meridional circulation increases in intensity. This is due to the enhanced surface heating in the cyclonic wind-driven gyre with the Ekman upwelling and the accompanying enhanced surface cooling in the deep water formation region. In the cyclonic wind-driven gyre, the Ekman upwelling brings up the thermocline to the subsurface depths to enhance the surface heating and also the downward heat conduction from the sea surface to the deep layer, which leads to warming of the deep water. Thus, the enhanced surface heating in the cyclonic gyre is balanced with the enhanced surface cooling in the deep water formation region due to the warmed deep water. In this way, the wind forcing enhances a thermohaline circulation, a wind-enhanced thermohaline circulation, which connects the deep water formation region to the cyclonic wind-driven gyre with the Ekman upwelling. In fact, a wind-enhanced thermohaline circulation can be seen both in the Pacific and the Atlantic. For the Pacific, the buoyancy flux through the sea surface for the cases with and without wind forcing in the North Pacific model of chapter 2 is depicted in Fig. 5.1. In the case with wind forcing, buoyancy is given to the ocean through the sea surface at high latitudes. There is a large buoyancy input to the ocean in the equatorial region, where the wind-driven upwelling also exists. Part of the buoyancy gain is used to compensate the buoyancy loss in the subtropical gyre, and the rest is used to enhance the upper part of the layered thermohaline circulation in the Pacific. For the Atlantic, difference of the surface heat flux between cases with and without wind forcing over the Southern Ocean in the world ocean circulation model of Hasumi and Suginohara (1998) is shown in Fig. 5.2. Wind forcing over the Southern Ocean intensifies both surface heating in the Atlantic sector of the Southern Ocean and surface cooling in the northern North Atlantic. Thus, the wind forcing over the Southern Ocean enhances the deep thermohaline circulation in the Atlantic associated with the formation of NADW.

Finally, the deep Pacific circulation has been investigated in an idealized two-basin model. Depth-dependent vertical diffusivity is employed to control the circulation. Vertical diffusivity estimated from observation is adopted for the upper layer ($0.1\,\mathrm{cm^2\,s^{-1}}$; e.g., Ledwell et al., 1993) and for the deep layer ($3.0\,\mathrm{cm^2\,s^{-1}}$; e.g., Morris et al., 1997). Comparison is made among the cases with different vertical profiles of vertical diffusivity at mid-depths, where the value of vertical diffusivity is not well known. When vertical diffusivity is set to increase with depth beginning at the lower thermocline depths, the deep Pacific circulation is significantly intensified with the enhanced deep and bottom water formation both in

the northern North Atlantic and the Weddell Sea. This is due to enhanced heat exchange between the lower thermocline water and the deep water through the enhanced diffusion at the lower thermocline depths. The water below the thermocline is warmed and the upper layer water is cooled for the whole basin. The warmed deep water leads to the enhanced deep water formation in the deep water formation region due to the excess heat loss through the sea surface. The cooled upper layer water leads to the excess heat gain through the sea surface, balancing with the excess heat loss in the deep water formation region. The deep water upwelled to the lower thermocline depths does not further upwell to the sea surface due to the small upper-layer vertical diffusivity but it flows back to the Southern Ocean slowly upwelling at the thermocline depths. In this way, the meridional overturning with large transport forms below the lower thermocline in the Pacific. This circulation yields tracer distributions that are well compared with the observation. Intensification of the deep Pacific circulation does not occur for the cases where vertical diffusivity is set to increase with depth beginning in the deep layer and where it is taken large at the lower thermocline depths but is not increase below that depths. Thus, it is found that to realistically reproduce the deep Pacific circulation, vertical diffusivity needs to be depth-dependent, the large value of $1.0\,\mathrm{cm^2\,s^{-1}}$ at the lower thermocline depths and the larger value of $3.0\,\mathrm{cm^2\,s^{-1}}$ in the deep layer. The deep Pacific circulation is considered to be the classical thermohaline circulation where its strength is strongly dependent on vertical diffusivity. This makes a remarkable contrast to the deep Atlantic circulation associated with NADW formation, which is the wind-enhanced thermohaline circulation (chapter 3; Tsujino and Suginohara, 1998) as demonstrated by Hasumi and Suginohara (1998).

When vertical diffusivity larger than $1.0\mathrm{cm^2\,s^{-1}}$ is taken in the deep layer, a set of alternating zonal jets, the stacked jets, along the equator is formed by the effect of vertical diffusion. The speed of the stacked jets is the greatest when vertical diffusivity increases with depth beginning at the lower thermocline depths. Since recent observations show that vertical diffusivity in the bottom layer is large (e.g., Toole et al. 1994; Polzin et al., 1997), it is considered that the stacked jets can be explained as part of thermohaline circulation (Suginohara and Fukasawa, 1988; Suginohara and Aoki, 1991).

The thermohaline circulation in the Pacific has not been extensively investigated as the Pacific is the terminal of the global conveyer belt circulation (Broecker, 1985; Gordon, 1986), nothing but the place where deep water is slowly upwelling. However, in the present

thesis, it is shown that the thermohaline circulation in the Pacific has various aspects and deserves more attention. It is important to take into account thermohaline effects to understand behavior of North Pacific Intermediate Water and Antarctic Intermediate Water. The mid-depth thermohaline circulation is enhanced by wind forcing, forming a meridional circulation connecting the Southern Ocean and the subpolar gyre in the North Pacific. The deep circulation in the Pacific is strongly controlled by depth-dependent vertical diffusivity, which evokes urgent need for thorough understanding of vertical diffusivity. Also an exact estimation of the formation rate of Atlantic Bottom Water in the Weddell Sea and other marginal seas around the Antarctica is needed.

In future, in order to understand the behavior of intermediate water masses such as NPIW, the more exact reproduction of the upper layer circulation for the North Pacific is essential: the effects of sea ice formation in the Okhotsk Sea, the water mass exchange through the Kuril Islands, the separation of the Kuroshio, and the mixing due to mesoscale eddies should be represented in the model. For the understanding of deep Pacific circulation, more extensive studies that can yield spatial distribution of vertical diffusivity and the formation rate of bottom water in the marginal seas of the Southern Ocean are strongly required.

References

Broecker, W. S., D. M. Peteet and D. Rind (1985): Does the ocean-atmosphere system have more than one stable mode of operation?, *Nature*, **315**, 21–26.

Gordon, A. L. (1986): Interocean exhange of thermocline water, *J. Geophys. Res.*, **91**, 5037–5046.

Hasumi, H. and N. Suginohara (1998): Atlantic deep circulation controlled by heating in the Southern Ocean, *Geophys. Res. Lett.*, submitted.

Ledwell, J. R., A. J. Watson and C. L. Law (1993): Evidence for slow mixing across the pycnocline from an open-ocean tracer-release experiment, *Nature*, **364**, 701–703.

Morris, M., N. Hogg and W. B. Owens (1997): Diapycnal mixing estimated from advective budgets in the deep Brazil Basin, in *International WOCE Newsletter*, No. 28, 23–28.

Polzin, K. L., J. M. Toole, J. R. Ledwell and R. W. Schmitt (1997): Spatial variability of turbulent mixing in the abyssal ocean, *Science*, **276**, 93–96.

Suginogara, N. and S. Aoki (1991): Buoyancy-driven circulation as horisontal convection on β-plane, *J. Mar. Res.*, **49**, 295–320.

Suginohara, N. and M. Fukasawa (1988): Set-up of deep circulation in multi-level numerical models, *J. Oceanogr. Soc. Japan*, **44**, 315–336.

Talley, L. D. (1993): Distribution and Formation of North Pacific Intermediate Water., *J. Phys. Oceanogr.*, **23**, 517–537.

Toole, J. M., K. L. Polzin and R. W. Schmitt (1994): Estimates of diapycnal mixing in the abyssal ocean, *Science*, **264**, 1120–1123.

Tsujino, H. and N. Suginohara (1998): Thermohaline circulation enhanced by wind forcing, *J. Phys. Oceanogr.*, in press.

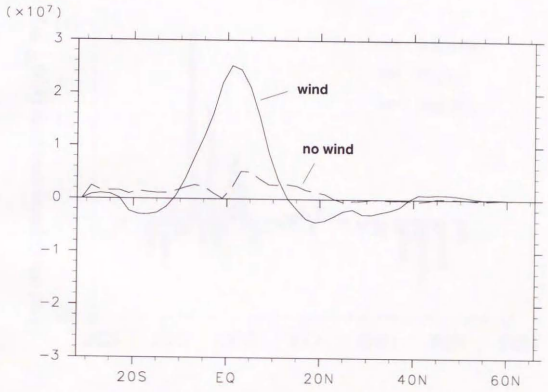

Figure 5.1: Zonally averaged buoyancy flux through the sea surface for the cases with and without wind forcing in the North Pacific model of chapter 2. The unit of the ordinate is $\sigma_\theta \cdot s^{-1}$. The positive values indicate buoyancy gain by the ocean (i.e., ocean is heated by the atmosphere).

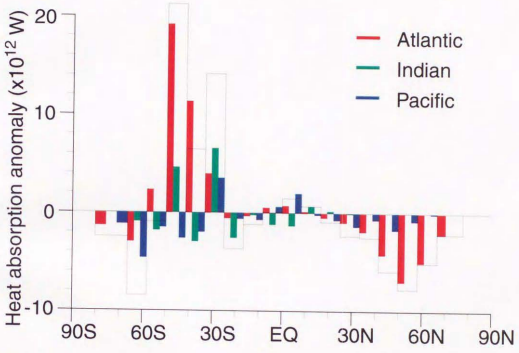

Figure 5.2: Annual mean surface heat flux anomaly caused by wind stress over the Southern Ocean ("effect" of wind stress over the Southern Ocean on heat flux through the sea surface) obtained by Hasumi and Suginohara (1998). Each box shows heat absorbed by the ocean in the latitudinal band indicated by the width of the box. Figure is taken from Hasumi and Suginohara (1998).

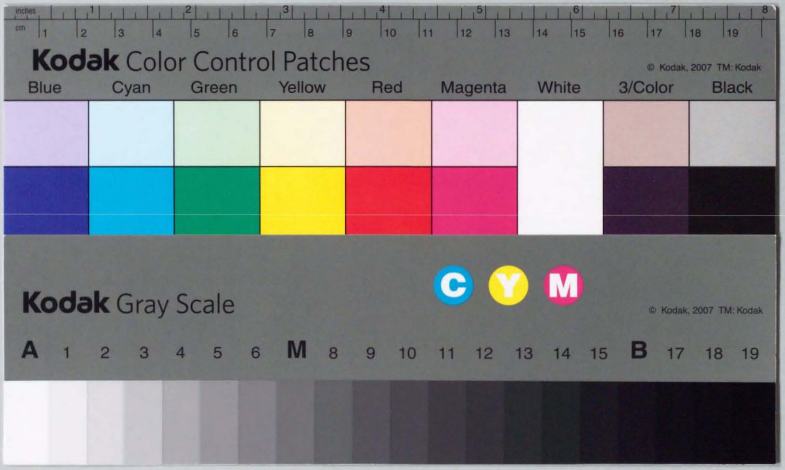
inches
cm
Kodak Color Control Patches
© Kodak, 2007 TM: Kodak
Blue
Cyan
Green
Yellow
Red
Magenta
White
3/Color
Black
Kodak Gray Scale
C
Y
M
© Kodak, 2007 TM: Kodak
A 1 2 3 4 5 6 M 8 9 10 11 12 13 14 15 B 17 18 19